Theoretical prediction of electric vehicle energy consumption and battery state-of-charge during arbitrary driving cycles

Theoretical Prediction of Electric Vehicle Energy Consumption and Battery State-of-Charge During Arbitrary Driving Cycles

by L. A. M. van Dongen (Eindhoven University of Technology), R. van der Graaf (Eindhoven University of Technology), W. H. M. Visscher (Eindhoven University of Technology) and H. C. J. Zeegers (Eindhoven University of Technology).

Battery State of Charge Model for Driving Cycle Operation [1])

by W. Visscher and L. A. M. van Dongen[2])

ABSTRACT

The actual performance of an electric vehicle depends on the capability of the battery to meet the power requirements of the drive train. In order to predict the vehicle operating range an accurate battery model is required. The behaviour of a battery depends on its state of charge. In the definition of the state of charge the characteristic relationship between available capacity and current must be accounted for. A voltage-current relationship is derived based on the polarization behaviour of a lead acid battery. This equation expresses the battery voltages as a function of current and state of charge. The theoretical equation is verified with data experimentally established at a 6 V battery. A program is written that calculates the cumulative charge reduction during driving cycle operation. This gives the state of charge as the driving cycle proceeds. By combining this with the relationship between voltage, current and state of charge, the battery voltage during the total driving cycle can be determined.
Battery voltage and energy are thus calculated for several types of driving cycles. These results will be compared with experimental data at a 6 V battery.

1. INTRODUCTION

The actual performance of an E.V. depends on the capability of the battery to meet the power requirements of the drive train. Operating modes differ widely and the vehicle characteristics vary with each model. Therefore, normalized drive cycles were proposed based on analysis of traffic patterns and several duty cycles are now in use to test battery performance for a given type of vehicle. Several attempts have been made to give also a model for the battery. Due to the chemical and physical processes that occur in the battery, its behaviour is more difficult to describe by an accurate model; moreover the battery characteristics change with time.
With models for the components of the drive train and the battery, computer simulation can be carried out to study the interaction of battery and drive train and to predict energy use, vehicle performance and operating range.
This paper will describe a battery model and compare calculated state of charge values with experimental data.

2. THE STATE OF CHARGE

The amount of energy that the battery can deliver is determined by its current-voltage characteristic which in turn depends upon the state of charge.
The state of charge of a fully charged battery is well defined; the concept of complete discharge depends on the discharge current due to the fact that in a battery the available capacity decreases with higher current. Hence the state of charge (S) at time t during discharge with current I must be related to the capacity (C_I) at current I [1].

$$S = 1 - \frac{I\,t}{C_I} \tag{1}$$

With the Peuckert relation

$$I^n \star \tau = \text{constant} \tag{2}$$

where τ = time required for complete discharge at current I
n = number, depending on the battery type,
$1.2 < n < 1.4$

C_I can be expressed in the capacity (C_N) at standard rate (I_N)

$$C_I = C_N \left(\frac{I_N}{I}\right)^{n-1} \tag{3}$$

The state of charge at any current is then related to the standard capacity with

$$S = 1 - \frac{It}{C_N}\left(\frac{I}{I_N}\right)^{n-1} \tag{4}$$

3. BATTERY DISCHARGE MODEL

Mathematical models for porous electrodes have been developed to describe the extent of utilization of a battery plate as a function of rate of discharge, involving structural changes during the discharge process [2, 3, 4, 5]. These are derived from the kinetic relationship between current density and electrode potential, taking into account mass transfer processes.
The complete battery behaviour is often described by the current-voltage relationship of Shephard [6].

[1]) Paper gepresenteerd tijdens 'Drive Electric' 1982 te Amsterdam.
[2]) Eindhoven University of Technology, Eindhoven, The Netherlands

$$E = E_s - K\frac{Q\,I}{Q - It} - R_E\,I \qquad (5)$$

in which
K = polarization parameter
Q = amount of available active material
R_E = electrolyte resistance
E_s = constant voltage

This equation has been derived assuming a linear relationship between current and potential at both electrodes. However, such a behaviour is a priori restricted to very low polarization conditions. Moreover, to fit the experimental data with eq. (5) a negative value of the resistance had to be chosen. This inconsistency was recognized by Shephard and attributed to the empirical nature of the equation.

During discharge with electric vehicle duty cycles high polarization conditions will prevail. Therefore a current-voltage relation will be derived which is applicable to high current discharge.

At the two electrodes 1 and 2 of the battery the discharge process takes place via cathodic reaction at electrode 1 and anodic reaction at electrode 2; this can be expressed by the general electrochemical rate equations.

at electrode 1 : $p\,OX_1 + ne^- \rightarrow p'\,RED_1$

at electrode 2 : $q\,RED_2 \rightarrow q'\,OX_2 + ne^-$

where OX_1 and RED_2 stand for the concentration of dissolved species at electrode 1 and 2 respectively.
p, p', q, q' = stoichiometric coefficients
n = number of electrons

At the two electrodes of the Pb acid battery these processes are:

at electrode 1: $PbO_2 + 3\,H^+ + H\,SO_4^- + 2\,e^- \rightarrow PbSO_4 + 2\,H_2O$

at electrode 2: $Pb + HSO_4^- \rightarrow PbSO_4 + H^+ + 2\,e^-$.

Under the conditions that the electron transfer occurs rapidly and that mass transfer to and in the pores of the electrode limits the rate of the reaction, the overpotential (η) for the reaction at electrode 1 is given by

$$\eta = \frac{RT}{nF}\ln\left(\frac{c_{OX,\,t}}{c_{OX,\,t=0}}\right)^p \qquad (6)$$

and similarly at electrode 2

$$\eta = -\frac{RT}{nF}\ln\left(\frac{c_{RED,\,t}}{c_{RED,\,t=0}}\right)^q \qquad (7)$$

where: η = overpotential [V]
R = gas constant [J.mol^{-1} K^{-1}]
T = absolute temperature [K]
F = Faraday constant [C mol^{-1}]
n = number of electrons

For a battery plate the concentration term $c_{OX,\,t=0}$ can be considered to be equivalent to the total amount of charge that is available at the fully charged plate 1, whereas $c_{OX,\,t}$ is the charge remaining after discharge with current I during time t, so

$$c_{OX,\,t} = c_{OX,\,t=0} - It \qquad (8)$$

With $C_{I,1}$ = capacity of electrode 1 at current I we have

$$\frac{c_{OX,t}}{c_{OX,t=0}} = 1 - \frac{It}{C_{I,1}} \qquad (9)$$

i.e. $\frac{c_{OX,t}}{c_{OX,t=0}}$ represents the state of charge $S_{I,1}$ of electrode 1.

Similarly $\frac{C_{RED,t}}{C_{RED,t=0}} = S_{I,2}$ of electrode 2.

The total cell voltage (E) during discharge is given by the algebraic sum of the two electrode polarizations:

$$E = E_{eq,\,1} + \eta_1 - (E_{eq,\,2} + \eta_2) - I\,R_E \qquad (10)$$

in which $E_{eq,\,1,2}$ = equilibrium potential of the electrode reaction 1, respectively 2
R_E = electrolyte resistance.

If both electrodes have the same capacity $C_{I,1} = C_{I,2}$ then $S_1 = S_2 = S$ and we can write for eq. (10) with substitution of (6), (7), (9).

$$E = E_{s=1} + \frac{(p+q)}{2}\frac{RT}{F}\ln S - I\,R_E \qquad (11)$$

where $E_{s=1} = E_{eq,\,1} - E_{eq,\,2}$

i.e. the cell voltage of a fully charged battery and determined by the H_2SO_4 concentration.
The electrolyte resistance R_E is in principle a function of the state of charge.

Eq. (11) describes the cell voltage during discharge with current I in dependence of the state of charge. It should be noted that this equation is restricted to high polarization conditions and hence is not valid at very low current or at I = 0.

To establish the parameters of eq. (11) discharge curves were recorded at a Pb acid battery at various I. The battery was a Varta electric vehicle battery, 6 V, type 240-15 with nominal capacity C_5 = 180 Ah. Capacity measurements as function of I gave a value of n = 1.26 for the Peuckert relation (2).
After each discharge the battery was charged with 20 A and finally with 6 A until the specific gravity was constant. From the data E-I plots were constructed at constant S, with S calculated according to eq. (4). This is represented in **Fig. 1**.

Fig. 2 shows the electrolyte resistance as a function of the state of charge measured by discharging the battery at C_5 rate to decreasing states of charge.
When the results of Fig. 1 are represented as a plot of E vs. ln S (**fig. 3**) a linear relationship is obtained and the slope of the curves is independent of the current. This is in agreement with eq. (11). The observed slope was found to be 0.26 V. About the same value was found when voltage - state of discharge plots given by Schleuter [7] for a tubular battery were replotted.
Fig. 2 shows that R_E does not vary significantly for $1 > S > 0.6$, so from eq. (11) it would follow that the slope of the E-I plot for high S is independent of S and is equal to R_E.
Though the experimental lines are indeed parallel, the slope is about $2 \times R_E$. (At S = 1 R_E = 1.37 mΩ). This can be explained by the resistance of the electrolyte in the pores which

is not measured during steady state experiments of fig. 3 but will contribute during actual discharge.

The above results show that the discharge behaviour at high polarization can indeed be described by a rather simple relationship.

4. STATE OF CHARGE OF THE BATTERY DURING DUTY CYCLE OPERATION

4.1. Model

When the discharge of a battery takes place along the pattern of a duty cycle, the current changes rapidly, moreover regenerative braking is involved. To account for this the state of charge must be calculated for small time intervals Δt during which I is considered to be constant, hence during discharge:

$$S = 1 - \frac{I\,\Delta t}{C_N}\left(\frac{I}{I_N}\right)^{n-1} \tag{12}$$

whereas during charge the incremental change of state of charge (ΔS) during a period Δt_c is given by [1]

$$\Delta S = \frac{I_c\,\Delta t_c}{C_{I_d}} \tag{13}$$

or with (2)

$$\Delta S = \frac{I_c\,\Delta t_c}{I_d\,\Delta t_d}(1 - S) \tag{14}$$

(Subscript c, d refers to charge respectively discharge).

A computer program was written to calculate the state of charge with eq. (11) and (13) after discharge with a given duty cycle, using the experimentally established E—I curves at constant S. The program calculates also the cell voltage and current during the duty cycle.

4.2. Battery power schedules

These simulation results were compared with the actual battery performance during duty cycle operation. The load cycle experiments were carried out at a 6 V battery with a machine convertor, consisting of an induction machine coupled to a 20 V - 400 A DC machine [8].

The total battery requirement of a vehicle following a velocity profile was calculated for the vehicle being built by the Eindhoven Electric car group. The main drag forces to be overcome are given by

$$F_{st} = f_r\,g\,M + \frac{1}{2}\varrho\,C_x\,A\,v^2 \tag{15}$$

(Zie verder pag. 100)

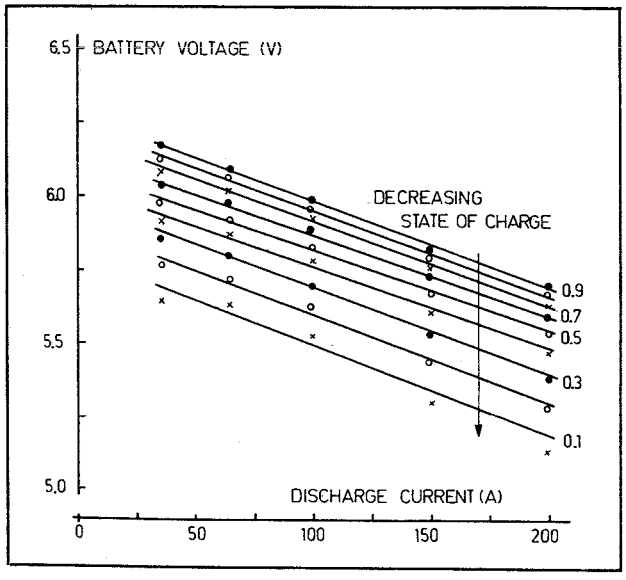

Fig. 1 Voltage-current characteristic during discharge as a function of state of charge

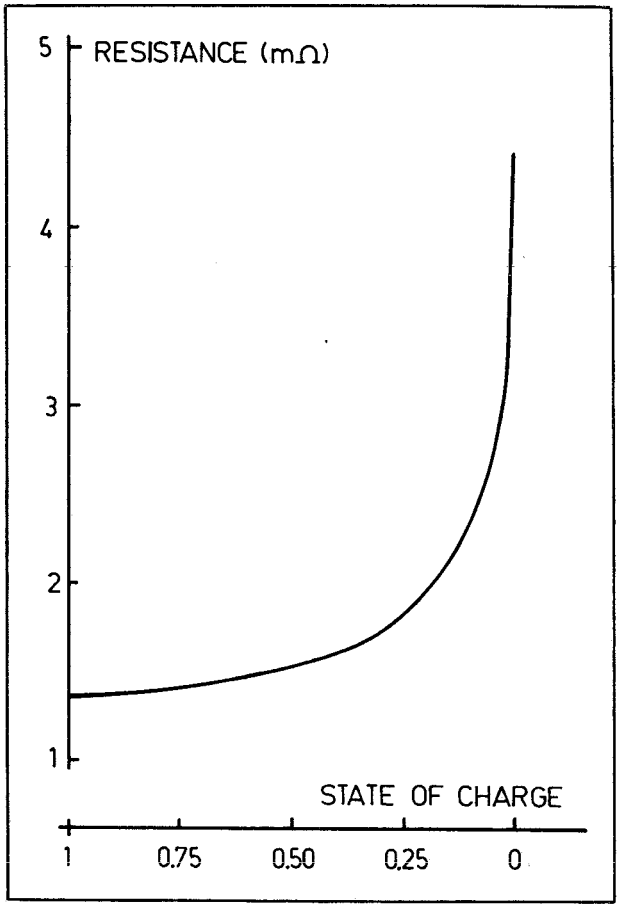

Fig.2 Electrolyte resistance of 6 V battery for decreasing state of charge

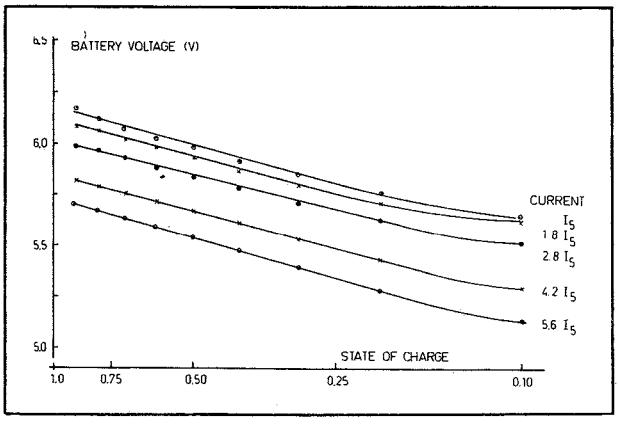

Fig. 3 Battery voltage vs. state of charge

where the parameters have the following meaning and specific value:

F_{st}	= drag force due to tire hysteresis and wind resistance	[N]
f_r	= coefficient of rolling resistance	(0.02)
g	= gravitational acceleration	(9.82 m s^{-2})
M	= vehicle mass	(1350 kg)
ϱ	= air density	(1.29 kg m^{-3})
C_x	= aerodynamic drag coefficient	(0.42)
A	= frontal surface area of the vehicle	(1.80 m^2)
v	= vehicle speed	[m s^{-1}]

Substitution of these values in eq. (15) gives

$$F_{st} = 264.87 + 0.488\ v^2 \qquad (16)$$

The total tractive effort of the vehicle (F_t) is equal to:

$$F_t = F_{st} + F_a = 264.87 + 0.488\ v^2 + M\ a \qquad (17)$$

F_a	=accelerating force	[N]
a	=vehicle acceleration	[m s^{-2}]

The wheel power requirement (in Watt) can be represented as

$$P = [264.87 + 0.488\ v^2 + M\ a]\ v \qquad (18)$$

Starting from this equation, the battery power has been determined assuming the average motor and gearbox efficiency to be 80 and 90% respectively.
The battery behaviour was investigated during three types of duty cycles viz. the European cycle, the SAE J 227 aD cycle and the THE cycle. The first two cycles are standard velocity versus time profiles; **fig 4** and **5** show the power profiles, calculated for the total battery pack (144 V).

The THE cycle was chosen as a representative of actual duty cycles, which have been recorded in typical Dutch cities with the aid of a DAF 31 outfitted with speed sensors and torque transducers at the rear wheel axles. Conversion of the results with respect to the estimated mass and drive train efficiency of the Eindhoven Electric Vehicle resulted in the battery power for the total battery pack profile indicated in **fig. 6.** The duration of one cycle is 20 minutes in contrast with the usually shorter cycle time of the standard duty cycles. Table 1 summarizes some duty cycle specifications.

Table 1. Duty cycle specifications

	EUR.	SAE J 227 aD	THE
Average vehicle energy [Wh/km]	145	189	140
Average vehicle speed [km/hr]	18 3	44 7	24 3
Distance covered per cycle [km]	1 010	1 516	8.1
Duration of 1 cycle [s]	198	122	1200
Stops/km	3	0.66	9
Idling time [%]	29 3	20.49	10.54
Charge recuperation / total discharge [%]	19 4	10	22.2

4.3. Voltage-current characteristics

E-I diagrams at constant S for the charging process were obtained from constant charging curves at various I starting with a battery discharged to S = 0 with I_5. The results, given in **fig. 7,** represent only the E-I curves for which the charge efficiency is 100%. Due to concurrent water electrolysis, the charge efficiency becomes less than 100% for E ≥ 2.35 V per cell. To account for this in eq. (13) the charge efficiency factor must be introduced and E-I plots for S > 0.6 will be presented later.

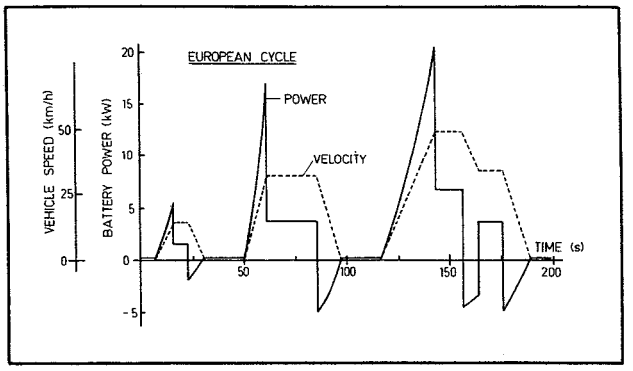

Fig. 4 Battery power and vehicle speed for European duty cycle

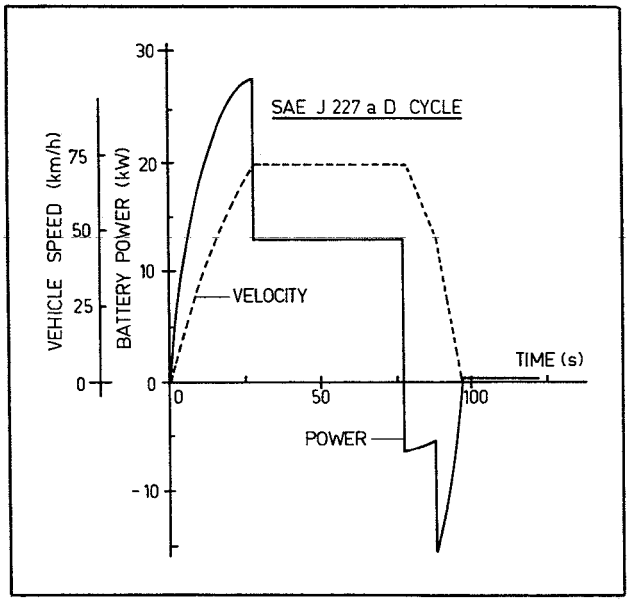

Fig. 5 Battery power and vehicle speed for SAE J 227 aD duty cycle

4.4. Comparison of test- and simulation results

The European and SAE J 227 aD cycle tests

To avoid the voltage range where charging might be inefficient, the calculation of the battery performance during the European and the SAE J 227 aD duty cycle was started at S = 0.6. This was experimentally realized by discharging the battery (Varta electric vehicle battery 6 V, 240.15 nominal capacity C_5 = 180 Ah), during 2 hr at C_5 rate. The battery was then subjected to a number of cycles (European or SAE) and thereafter the rest capacity (C_R) was measured at the C_5 rate.

Results:

	Experimental	Calculated
European cycle		
Netto discharge during 60 cycles (Ah)	59.8	63.1
C_{Rest} (Ah)	36.0	35.1

SAE J 227 aD cycle		
Netto discharge during 30 cycles (Ah)	65.5	66.5
C_{Rest}	24.0	13.8

The experimental and calculated voltage and profiles during the 60th European cycle and during the 30th SAE cycle are given in **fig. 8** and **9** respectively.

The battery voltage during discharge agrees within 0.1 V with the computed value but the experimental data during charging are lower, indicating a retarded battery respons such that very rapid current changes are less effective.

Calculation of the state of charge shows that S = 0 will be reached after 55 SAE cycles, i.e. an operating range of 83 km. This is in agreement with the experimental observation that the discharge could be continued during about 53 cycles before the power delivered by the battery at the highest discharge peak was 10% less than demanded by the duty cycle.

THE cycle tests

The average current of the THE cycle is ca. 33 A, the maximum current during discharge is ca. 200 A, during charge 160 A.

The battery could meet the duty cycle demands during 13 cycles (i.e. operating range 105.3 km).

After the battery had been discharged with 13 cycles C_R was

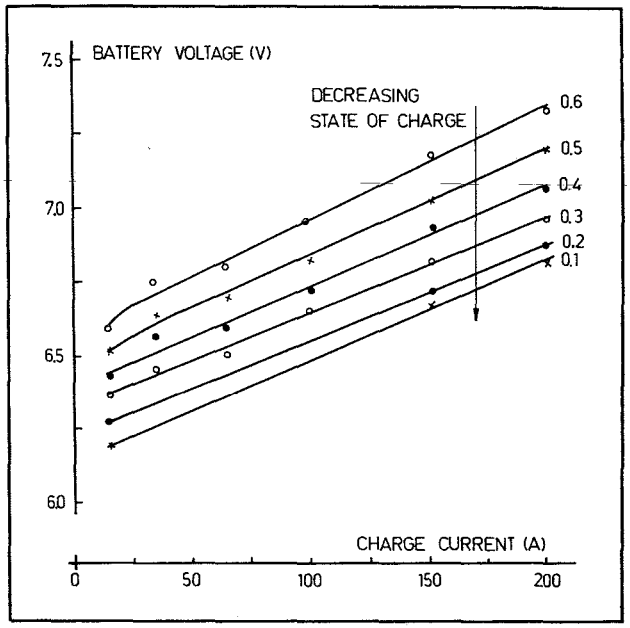

Fig. 7 Voltage-current diagram during charging as a function of state of charge up to S = 0.6

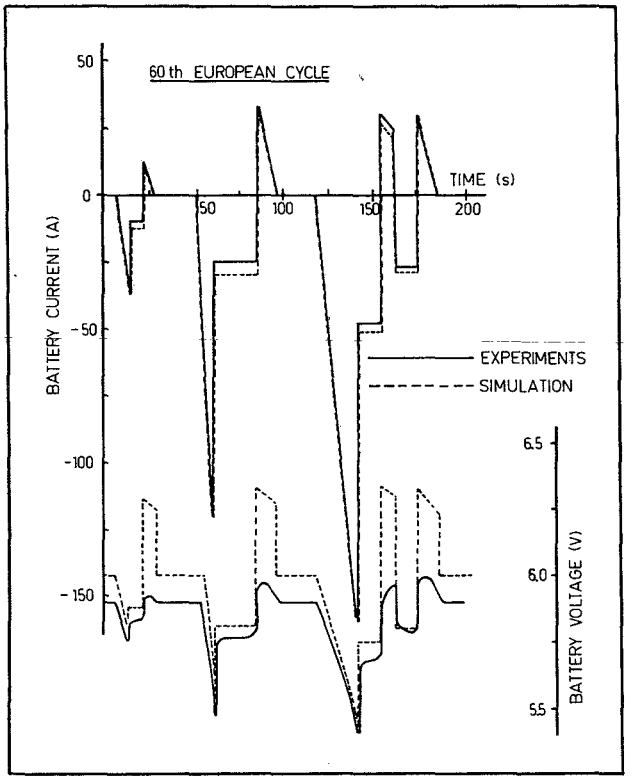

Fig. 8 Simulated and experimental battery voltage and current profile during 60th European cycle

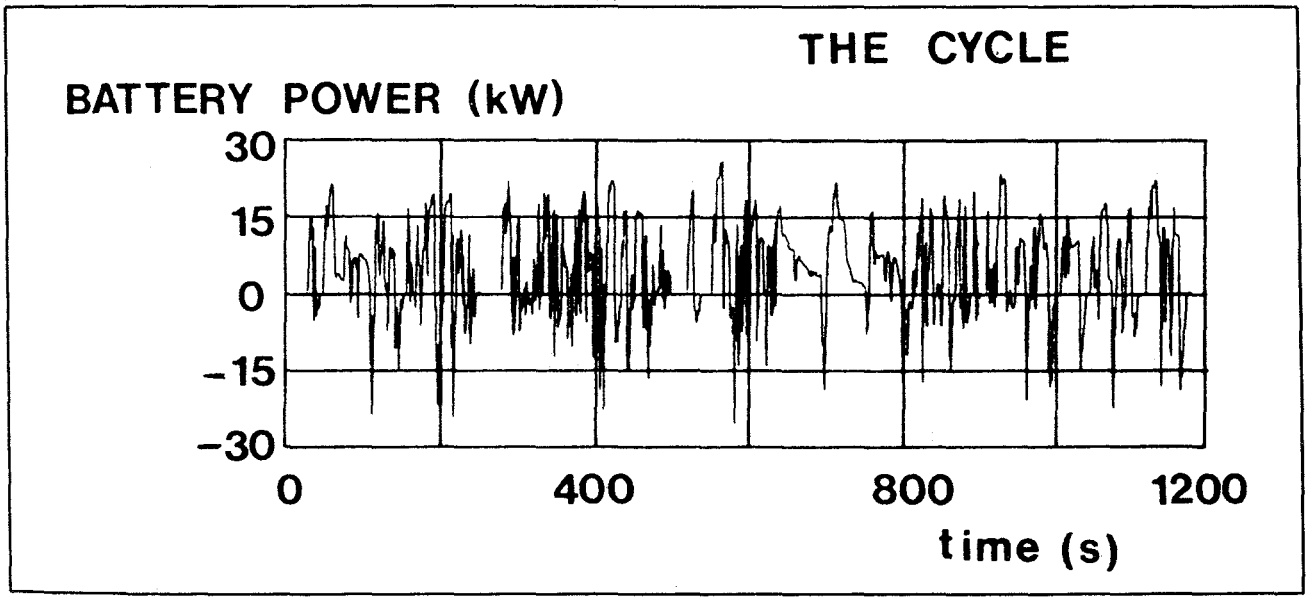

Fig. 6 Battery power for THE duty cycle

determined at C_5 rate. The experimental C_R was found to be 31 ± 5 Ah, while the calculated C_R was 19.2 Ah.
Fig. 10 shows the cell voltage (E_D) at the highest discharge peak and the cell voltage (E_C) at the highest charge current peak during 13 cycles and the cell voltage E_R at I = 0 at the end of each cycle. In the figure the computed data are given from 8th to 13th cycle.

5. CONCLUSIONS

The effect of state of charge of a battery upon the current voltage characteristics was described by a simple relation. Calculation of the state of charge during duty cycle discharge was found to agree within 7% with experimental results and the actual battery voltage during electric vehicle operation agrees with the simulated performance.
With this model matching of power train and battery can be evaluated (9) and energy use and operation range can be predicted.

REFERENCES

[1] K. E. White, Society of Automotive Engineers, paper 78216

[2] D. Simonsson, J. Appl. Electrochem. 3, 261 (1973).

[3] W. Stein, Ph. D. Thesis, Aachen 1959.

[4] K. Micka and I. Rousăr, Collect. Czech. Chem. Commun. 40, 921 (1975).

[5] J. Newman and W. Tiedeman, Al Ch.E.J. 21, 25 (1975).

[6] C. M. Shephard, J. Electrochem. Soc. 112, 657 (1965).

[7] W. Schleuter, ETZ Archiv. Bd 4, 91 (1982).

[8] W. Visscher, W. de Zeeuw and R. van der Graaf, 5th International Electric Vehicle Symposium, Philadelphia 1978, paper 783107.

[9] L. A. M. van Dongen, R. van der Graaf and W. Visscher, 6th International Electric Vehicle Symposium, Baltimore 1981, paper 8115.

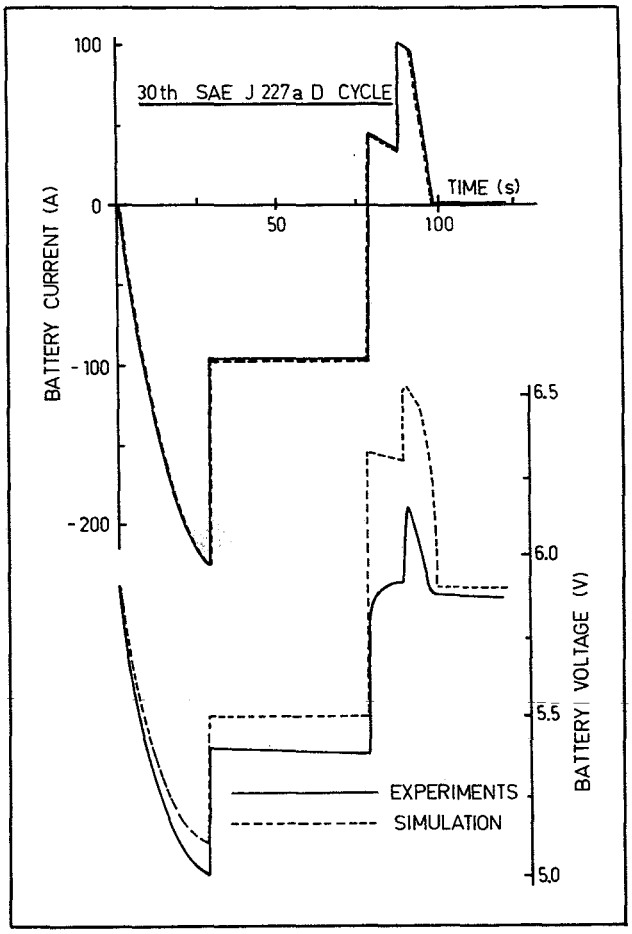

Fig. 9 Simulated and experimental battery voltage and current profile during 30th SAE J 227 aD cycle

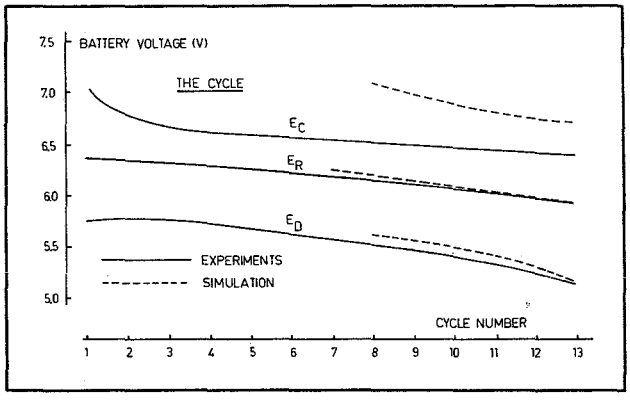

Fig. 10 Change in battery voltage at highest discharge current peak (E_D), at highest charge current peak (E_C) during 13 consecutive THE cycles and battery voltage at the end of each cycle (E_R)

The Eindhoven Experimental Electric Vehicle: Vehicle Design and Drive Train[1])

SUMMARY

At Eindhoven University of Technology a multidisciplinary team of chemical, electrical and mechanical engineers is collaborating on construction of an electric commuter car/van.
A VW-Golf which concept appears to be very suitable for this purpose, has been electrified. Car-body and rear suspension were modified thus that a rapidly exchangeable battery pack could be placed in a central box.
Various ways of controlling the powerflow from the 16/33 kW Siemens dc-motor to the wheels will be tested in this vehicle.
Three systems, which are under construction, are described:
- battery switching, field weakening and a fixed ratio transmission
- battery switching, field weakening and automatic gear-shifting
- fully electronic control by means of choppers.

by L. A. M. van Dongen and R. van der Graaf[2])

1. Introduction

During the last decade the importance of the development of electric road vehicles has widely been recognized. In the beginning much effort has been displayed on the construction of electrically driven buses and vans for a variety of reasons.

A group of interested persons at the Eindhoven University of Technology discerned the challenge which was put in this field by the passenger car as a replenishment of those activities. Especially in this application some features of the electric drive, such as battery weight, energy-efficiency of the drive line, selection and construction of components to be

[1]) Paper gepresenteerd tijdens 'Drive Electric 1982' te Amsterdam
[2]) Eindhoven University of Technology, Eindhoven, The Netherlands.

used, cost of these components, vehicle safety aspects, asked for a thorough investigation.
Optimization of a vehicle concept with respect to these features was considered necessary, and therefore a multi-disciplinary team was formed in which the chairs of Electrochemistry (Department of Chemical Engineering), Electromechanics (Department of Electrotechnical Engineering) and Transport Research (Department of Mechanical Engineering) are taking part.

On-the-road testing of various methods of motor control and types of battery would be an important part of the investigations.
It was expected that the project would give rise to a number of educationally very interesting studies for the final theses of postgraduate students, whereas the members of the multidisciplinary working group hoped to learn a lot from each other.
These expectations are largely being fulfilled.

2. Vehicle Concept

Specifications:
In an early stage the vehicle specifications of the Eindhoven Electric Vehicle (EEV) were set up:

- Top speed: 80 km/h
- Acceleration: 1.5 m/s^2 up to at least 50 km/h
- Operating range: 100 km
- Passenger capacity: 2 + 2 (two adults with two children or luggage)
- Rapidly exchangeable battery pack
- Distinct attention should be paid to the active (road-holding and vehicle handling characteristics) and passive safety (mechanical and electrical in the case of collision).

From these specifications the purpose of full compatibility of the EEV with normal urban and suburban traffic can be noticed. It will also be clear that the operational demands of this electric passenger car are strongly determined by the availability of electrochemical batteries. In fact the lead-acid battery still appears to be the only short term alternative for the independently moving road vehicle.
The restricted energy and power density and the excessive weight of this energy storage system are responsible for the limited speed, acceleration and operating range. For purposes of range extension and improvement of the battery service-ability it was decided to install a rapidly exchangeable battery pack in the vehicle.

Technical concept:
To obtain a reasonable range the battery weight will amount to about one third of the gross vehicle weight. The car will show proper steering characteristics if this large proportion of mass has a low centre of gravity with a good weight distribution over front and rear wheels and a moment of inertia that is as low as possible with respect to the vertical axis through the car's centre of gravity.
Hence it can be concluded that the batteries should be placed near the middle of the car.
Crash safety will also be favoured in this case, as the batteries and connectors are situated away from the outskirts of the vehicle.
These considerations, together with the required quick exchangeability of the battery pack, led to the concept of a central battery case in the floor of the car body. By integrating this case in the body a kind of backbone is created resulting in good structural strength and stiffness of the total construction.
This concept of a central battery case also facilitates meeting the already early discerned need for conditioning of the batteries [1].
This conditioning comprises:

- ventilating the battery compartment to remove the escaped hydrogen gas
- heating the batteries during winter time; in order to prevent dropping of the capacity to too low a level, the temperature should be kept above 15°C
- cooling the batteries when the temperature would reach too high a level; above about 50°C the active mass can deteriorate.

Selection and modification of a car:
After some preliminary design studies [2] it was decided to start from an existing passenger car or light van which would be modified in order to meet the requirements mentioned before. Thus a great deal of body engineering is avoided and the development efforts can be concentrated on propulsion systems and chassis modification on behalf of the battery pack.
In selecting a car the following criteria were applied:

- the car must have front wheel drive so that the voluminous battery case can readily be accomodated
- the rear wheel suspension should permit accomodating this case without drastic modification of this suspension
- the car should be able to carry the extra battery weight of some 5000 N with only minor changes; this implies that the gross vehicle weight will be at least 15000 N.
- sufficient room should be available between the front doors to accomodate the battery case and two seats
- the motor compartment should be able to house the different types of drive systems (see 3) that are to be tested.

It appeared that out of the small European cars the Volkswagen Golf fulfilled these requirements in the best way. Thus the EEV has been built upon this type.
With type and weight of the vehicle known, the power requirements of the drive train can be stated. To maintain the fully loaded vehicle at its required top speed of 80 km/h, the propulsion motor should have a continuous power output of at least 13 kW. Among the available electric motors the Siemens 1GV1, being a separately excited motor, especially developed for electric vehicles, fitted best into the specifications with:

- nominal power 17 kW
- maximum power 34 kW
- nominal speed 2200 rpm
- maximum speed 6700 rpm
- nominal voltage 130 V

With this motor the estimated acceleration of 1.5 m/s^2 can only de maintained until approximately 43 km/h; at higher velocities this value will gradually fall down.

In **Fig. 1** the top view of the changed car shows clearly the drive train, central battery case and modified rear axle.
According to the aim of testing various types of battery, the case has been constructed in such a way that batteries with different dimensions can be accomodated.
The batteries are placed in a wheeled sledge which can roll in the case and which is provided with sliding contacts at its front side.

The specifications of the first battery pack to be used, are:

type: Varta 240-15, EV battery
voltage: 20 x 6 V
capacity: 180 Ah at 5 h discharge

Maintenance of the original rear wheel suspension, trailing arms with an integral transversal anti-roll bar, would result in too high a battery pack location.
This construction has therefore been replaced by totally independent wheel suspension with newly constructed inner supports for the trailing arms.

3. Drive system and motor controller

General description:
Many passenger car manufacturers are developing and testing several drive systems in various electric vehicles. Due to different vehicle characteristics and testing conditions it is almost impossible to obtain a reliable comparison of these drive trains. Moreover, the near-term objective arises of optimizing drive systems using currently available components with respect to operating rang and primary energy consumption. For these reasons in the Eindhoven Electric Vehicle various drive systems are being constructed and tested under identical conditions.

The dc-series motor has long been regarded as an excellent choice for traction application because of its capability to deliver a large torque at low speeds. Control of the torque generated by the motor can be achieved by varying the magnitude of the supply voltage. A separately excited dc-motor, which provides the best combination of efficiency, performance and controlability for the near-term electric vehicle, is significantly different and has been chosen for the EEV. The speed of this motor can be controlled by field weakening in the speed range above nominal speed and by varying the armature voltage or circuit resistance in the speed range below nominal speed.
As a rule the motor is coupled to the propeller shaft by means of a step-down gear and the motor must therefore be capable of being adjusted over the entire speed range. Simulation studies, however, [3] demonstrate that from an energetical point of view a propulsion train using a variable transmission ratio has to be preferred to a drive system with a fixed gear ratio.

Fig. 2 Interior of the modified Golf, showing the battery case construction

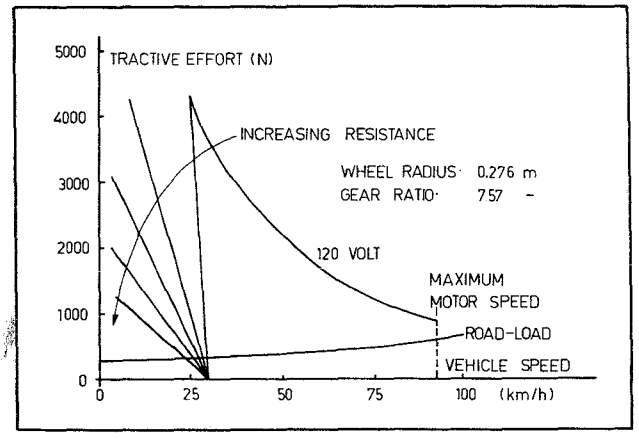

Fig. 3 Resistive motor control

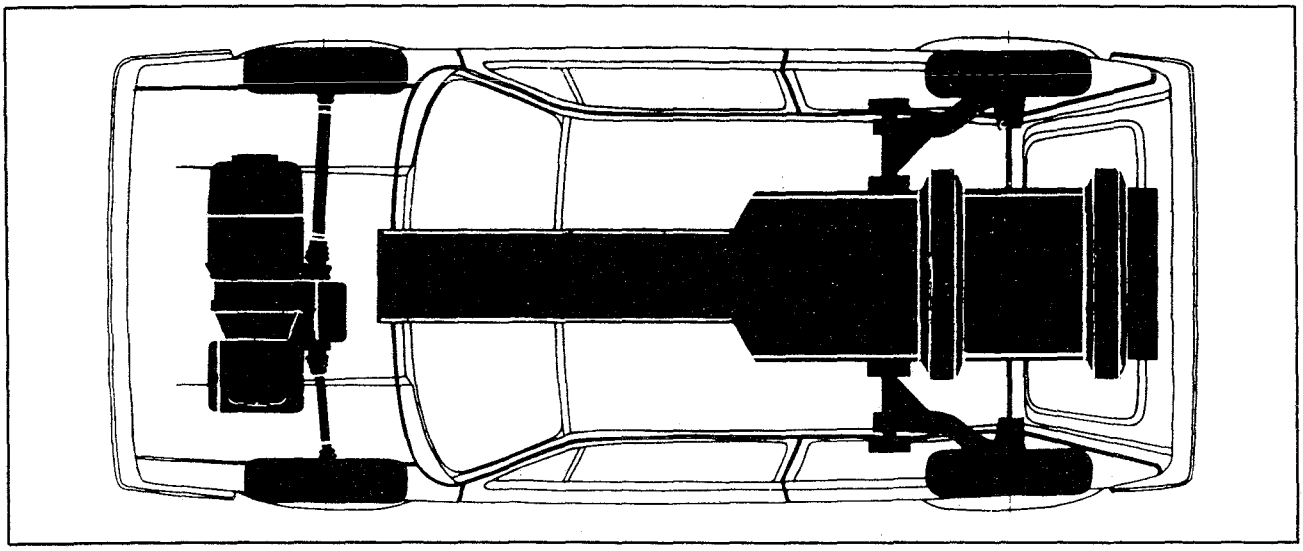

Fig. 1 Top view of modified car

In general, three areas of control can be discerned over the motor speed range:

1. **field weakening** in the upper part of the range.
As the field requires relatively low currents (up to 7 Amps approximately), field controllers are almost exclusively of the cheap single quadrant transistor-type.

As only a limited control range is realized by field weakening, further adjustment is necessary:

2. **adjustment of motor speed** can be performed in various ways:

- Continuously Variable Transmission
- Automatic gearbox
- Manually shifted gearbox
- Hydrostatic transmission

} motor control only by field weakening

- Battery voltage switching
- Armature current chopper (transistor or thyristor)

The fourth and sixth type permit adjustment from zero vehicle speed. The other types necessarily need:

3. **slipping devices** for starting from standstill
This function can be fulfilled by:
- resistive motor control
- friction type of coupling
- hydraulic coupling
- torque converter

In a preliminary study the control devices mentioned under points 2 and 3 have been reviewed and compared. The various possibilities have to be judged from different points of view, each of them delivering a number of criteria:

point of view	*criteria*
economical	cost
	energy efficiency
operational	reliability
	maintenance
	duration of life
vehicle handling	ease of operating
	smoothness
design	feasibility of optimal control
	feasibility of recuperative braking
	weight, dimensions, divisibility } of devices
environmental	noise

From these considerations it appeared to be desirable to construct and test three drive/control systems in the vehicle:

- voltage switching, field weakening and a fixed ratio transmission
- voltage switching, field weakening and automatic gear shifting
- fully electronic control by means of choppers.

In the first and second system also resistive control has to be comprised for low speeds.
In the following part the selected control systems will by described in more detail.

Resistive motor control
In the past this control has been the most popular type in use because of its low cost and quiet and smooth operation. At high vehicle speeds the field chopper is responsible for motor control and at low speeds resistors are switched into the armature circuit, as shown in **Fig. 3.** In order to provide a smooth operation a sufficient number of resistance steps is required. In the resistors, however, energy destined for propulsion is lost, and regenerative braking is impossible over this motor speed range. This greatly reduces the operating range in the typical type of driving of an electric vehicle: start and stop urban travel. The total amount of energy, which is lost in the resistors, can in fact be reduced by using a multi-speed gearbox, which allows the resistor to be switched out of circuit over a larger vehicle speed range. Because of the considerable energy losses in the resistors, purely resistive control does not deserve consideration for a modern electric vehicle.

Voltage switching
Another apparently simple form of speed control for an electric vehicle consists of a group of electric contacts in combination with some resistance elements. The battery pack is provided with several taps, at various voltages and the contacts reconnect the motor armature to various parallel and series combinations in order to give the appropriate motor voltage depending on desired speed. It is difficult to realize more than three or four acceleration steps, because the number of switching elements almost doubles with each step. Moreover, practical mechanical controllers are often extremely complex due to circuit demands, that are important for reasons of safety, and additional switching devices installed to ensure that all batteries are discharged uniformly.
An automatic voltage switching system has been designed, so that 30, 60 or 120 Volt is obtained at the motor terminals [4]. **Fig. 4** shows that the speed range ratio, that can be controlled by field weakening as stated above, has been quadrupled by simply changing the batteries from series to parallel connections. Only additional measures are required for bridging the start-up range. Although the system just described does provide control of speed, a complete covering of the tractive effort/speed range cannot be realized. Moreover, the tractive effort falls off, because voltage switching occurs at no-load conditions in order to prevent arcing of the switches.
In order to limit the armature current at low vehicle speeds a resistor can be used. This can also be realized in a simple way by using a hydrodynamic torque converter.
Although the damping characteristics of a torque converter

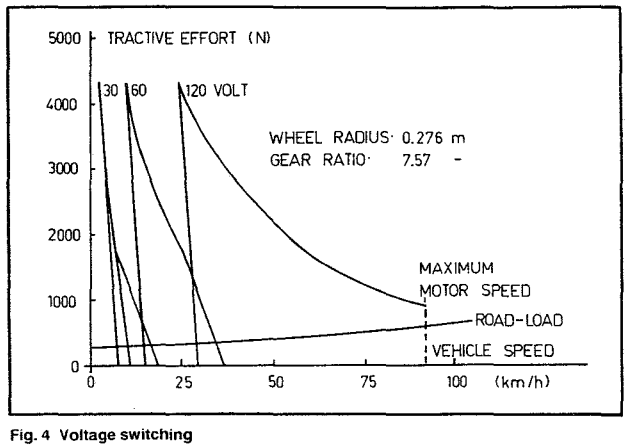

Fig. 4 Voltage switching

are attractive, it has tremendous energetical disadvantages [5]:

- torque converters have high losses in the converting range and a minimum slip of at least 2% occurs in the coupling range
- a torque converter requires an oil pump, the losses of which are high and proportional to the rotational speed.

For this reason a drive train having a fixed gear ratio of 7.57 and the dc motor controlled by a voltage switching system with a starting resistor is being tested in the vehicle now.
By mounting a multi-speed gearbox the number of unattainable operating points in the tractive effort-speed plane can considerably be reduced. The transmission ratios have to be matched in order that:

- as many as possible operating points can be adjusted
- an as high as possible average motor efficiency is realized
- gear changes and frequent speed variations in town traffic do not coincide.

In order to have an impression of the vehicle operating conditions in town traffic several driving cycles have been recorded in typical Dutch cities as The Hague and Delft. After analysis of these recordings and conversion of the results, curves of constant operating time have been constructed in the force-speed plane of the electric vehicle, as is indicated in **Fig. 5** [6].
For convenience of handling during city driving a standard automatic gearbox has been modified. In order to minimize the power losses in the gearbox, the torque converter has been replaced by a primary gear wheel reduction and the oil pump power has been optimized by using a separate constant speed oil pump instead of the standard oil pump. **Fig. 6** shows that the gear ratio of the primary reduction has been selected in such a way that gear changes only occur at less frequent operating points. The individual overall gear ratios stand at 16.58, 9.41 and 6.50 for the first, second and third gear respectively. Since the motor operates at speeds between 2200 abd 5500 rpm and the resistor is only switched in when the vehicle accelerates from standstill, high efficiency and sufficient operating range can be attained by this approach.
Due to motor synchronization during shifting procedures the operational comfort of the drive system is expected to be at least comparable with that of vehicles with an internal combustion engine and an automatic gearbox.

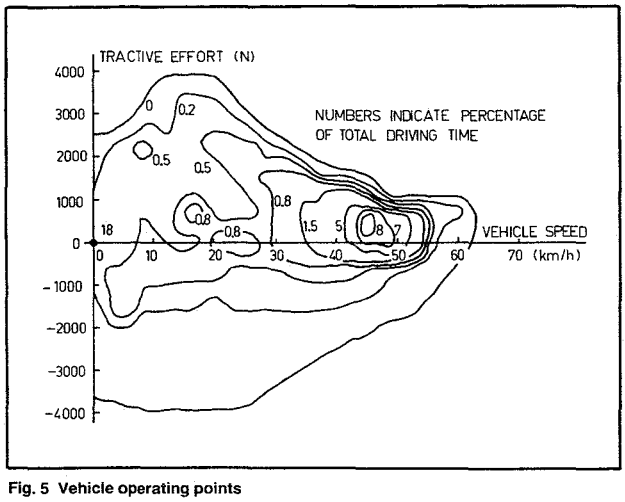

Fig. 5 Vehicle operating points

Fully electronic motor control
Another possible approach is to use an electronic switch in the armature circuit. The switching element is turned on and off at a certain frequency and thus has the effect of chopping the battery voltage.
In this way the armature voltage can be varied smoothly from 0 Volt to the full battery voltage by controlling the time intervals during which the switch is open. The chopper may roughly be regarded as a dc transformer. Since the losses in the chopper stand at about 4% of the power transmitted, the motor power nearly equals the power supplied by the battery. Without much extra expense these choppers allow regenerative braking in the entire speed range.
In principle it is possible to dispense with a multi-speed gearbox when a drive system with a dc motor and a dc chopper is used on the condition that the motor has been designed to handle the high currents drawn during the starting phase **(Fig. 7)**.

Due to the infinitely variable adjustment of the propulsion power a smooth speed control is realized. When the vehicle is moving at low speeds the field current stands at its maximum and speed is adjusted by varying the armature voltage with the chopper. At vehicle speeds requiring motor speeds higher than its nominal speed, the armature chopper applies

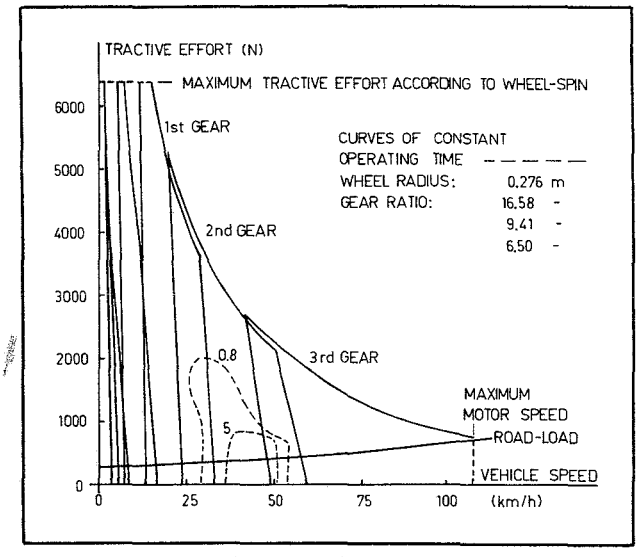

Fig. 6 Voltage switching and a multi-speed gearbox

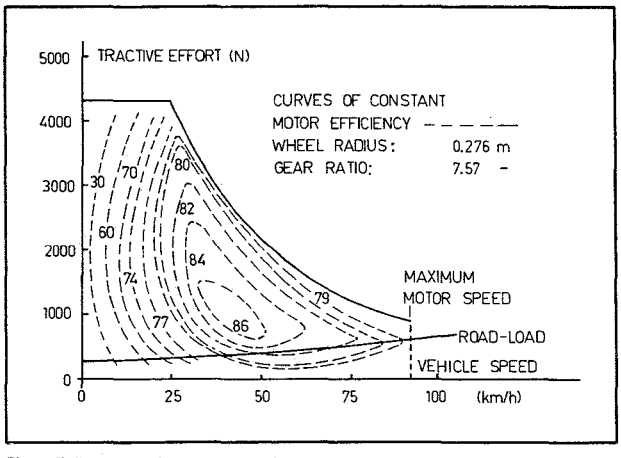

Fig. 7 Fully electronic motor control

full battery voltage to the motor terminals and the vehicle speed can be controlled by variation of the field current.
Yet the use of a multi-speed gearbox has the following advantages (**Fig. 8**):

- during the starting phase a higher gear ratio can be engaged, which reduces the initial current drawn from the battery
- with the possibility of selecting different gear ratios it is easier to meet demands for hill climbing
- since separately excited dc motors are less efficient at low rotational speeds, variable gear ratios allow highly efficient motor operation.

A thyristor chopper for the armature circuit is being developed which will control the Siemens motor coupled to either the step-down gear or the automatic gearbox.
The efficiency of these approaches appears to be high, since the losses in the motor controller are small and regenerative braking is possible. Other advantages are operational comfort and acceptable range. A disadvantage of these drive systems is the costly armature controller, which must be able to handle currents up to the 350 Ampere.

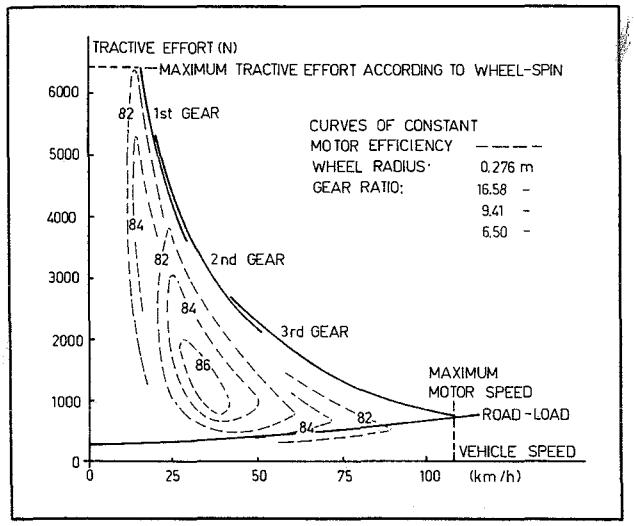

Fig. 8 Fully electronic motor control and a multi-speed gearbox

REFERENCES

[1] W. H. M. Visscher, W. de Zeeuw, R. van der Graaf: Experiments on Lead-Acid Batteries of an Electric Vehicle.
EVS-5 Philadelphia, Oct. 1978.

[2] W. A. Koumans: The Electric Car Project of the Eindhoven University of Technology.
PPL Conference Publication, no. 14.

[3] L. A. M. van Dongen, R. van der Graaf, W. H. M. Visscher: Theoretical Prediction of Electric Vehicle Energy Consumption and Battery State-of-Charge during Arbitrary Driving Cycles.
EVC Symposium VI, Baltimore, Oct. 1981.

[4] H. C. J. Zeegers: Torque control of a shunt wound dc-motor of an electric vehicle by means of continuous field control and stepwise adjustment of the armature voltage.
Drive Electric Amsterdam '82. Oct. 1982.

[5] Leo A. M. van Dongen: Efficiency Characteristics of Manual and Automatic Passenger Car Transaxles.
Society of Automotive Engineers, paper 820741. Troy, Michigan, June 1982.

[6] S. W. M. van Vuuren: Analyse van een stadsrit. Eindhoven University of Technology, Dept. of Mech. Eng. Internal report.

Torque control of a shunt wound DC motor of an electric vehicle by means of continuous field control and stepwise adjustment of the armature voltage [1])

ABSTRACT

It is shown that notching armature voltage and continuous field control can be a compromise solution for EV-drives. For the given vehicle parameters the necessarily series resistors are determined. An analysis of field control at different armature voltages is given for both stationary and dynamic conditions. Flow chart and block diagram of the control system are given. Attention is paid to the MOSFET-implemented field controllers and to the measurement of the electromagnetic torque using armature and field current.

by H. C. J. Zeegers [2])

1. Introduction

In the early seventies a group at the university of Eindhoven started to work on the subject of electrically driven vehicles in order to provide authorities with reliable data in this field. In 1973 it was decided to develop an electric passenger car.

1.1. The EV of the Eindhoven University of Technology

The vehicle should meet the following requirements [7]:

1. capacity: 2 adults + 2 children (so called 2+2 car);
2. range: 100 km;
3. topspeed: approx. 90 km/h;
4. cruising speed: 50-70 km/h;
5. acceleration: 1.5 m/S^2 up till 50 km/h;
6. gradients: 20% at stall condition;
7. rapidly exchangeable battery pack;
8. active safety (good road-holding, handling and suspension);
9. good passive safety considering the presence of the battery pack;
10. the electric drive should be such that it offers high efficiency and makes the car easy and pleasant to drive, also for persons used to cars with internal combustion engine. Besides that it should be cheap and servicing should be easy to be carried out by garage personnel with little extra training;
11. regenerative breaking.

After research by the groups transport research [3], [4] and electrochemistry [4], [10], it was decided to modify a VW-Rabbit car and equip it with a 120 V - 240 Ah lead-acid battery. The battery pack is made up of twenty 6 V-batteries. This concept resulted in a total vehicle weight of approximately 1500 kg.
Taking into consideration the requirements for the electrical drive (see point 10), it was concluded that while an armature-chopper has the advantage of easy control and good effi-

[1]) Paper gepresenteerd tijdens 'Drive Electric 1982' te Amsterdam.
[2]) Eindhoven University of Technology, Eindhoven, The Netherlands.

ciency, it has the disadvantage of being expensive and containing a lot of advanced electronics. It was expected that stepwise armature voltage adjustment with field control in addition would offer a good compromise solution. In order to verify this statement both systems should be investigated. The following program was started:

A. Development of a system based upon stepwise armature voltage adjustment by means of electromagnetic switches and continuous field control by a transistor chopper. At very low speeds additional armature resistors are required.

B. Development of a system with an armature **and** field current chopper.

C. Comparison of A. and B.

This paper deals with part A. of the project. To realize A. a fixed reduction between machine shaft and wheels of 7.6 had to be considered, which means that the machine speed must be controlled over a large range. Driving backwards is possible by reversing the field current. In order to realize regenerative breaking, with this circuit configuration it is best to use a DC-machine with separate excitation.

A Siemens-machine, type 1GV1 appeared to be the most suitable traction machine commercially available. Nominal and maximum values are specified in table 1 [9].

Mechanical and electrical performances are shown in **fig. 1a and 1b**.

TABLE 1

	Nominal	Maximum
Armature voltage	130 V (at nom.motor cond.)	180 V
Armature current	150 A	320 A (3 min)
Excitation voltage	100 V	—
Excitation current	7 A	—
Speed	2200 min^{-1}	6700 min^{-1}
Torque	75 Nm	160 Nm
Power	17 kW	33.5 kW

1.2. Speed control of the separately excited DC-machine

A seperately excited DC-machine offers two gates, named armature and field winding terminals, through which it can be controlled.

Fig. 2. shows a machine connected to a voltage source U and loaded with a torque T_L plus friction torque T_{fr}.

The total inertia of armature plus load is called J.

This drive can be described by the following equations:

$$U = I_a R_a + L_a \frac{dI_a}{d\tau} + E + \frac{I_a}{|I_a|} U_b \qquad (1)$$

$$E = c_m \Omega \Phi_a \qquad (2)$$

$$T_e = c_m I_a \Phi_a \qquad (3)$$

$$T_e = T_L + T_{fr} + J \frac{d\Omega}{d\tau} \qquad (4)$$

$$U_f = \frac{d\Phi_s}{d\tau} + I_f R_f \qquad (5)$$

Due to leakage, Φ_s and Φ_a differ slightly.

If we consider the system under quasi-stationary conditions ($\frac{dI_a}{d\tau} \approx 0, \frac{d\Omega}{d\tau}$ is small) and if we neglect the armature reaction and the voltage drop U_b across the brushes, which

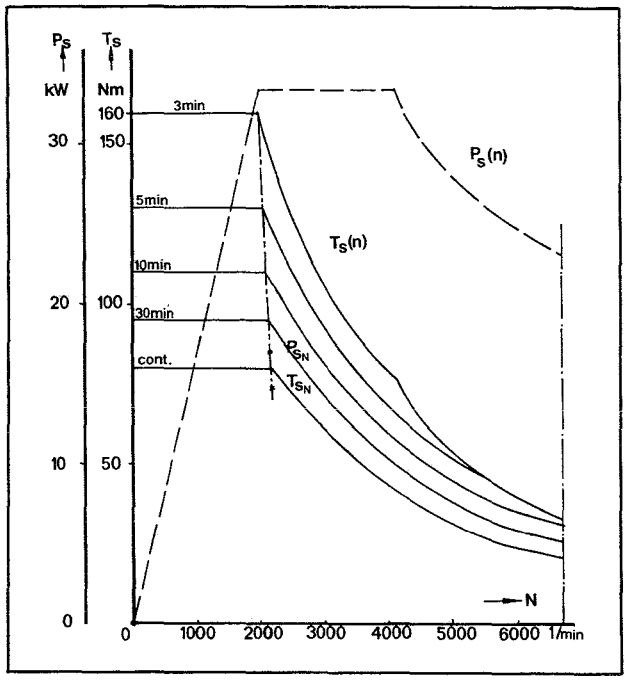

Fig. 1a The mechanical performances of the 1GV1

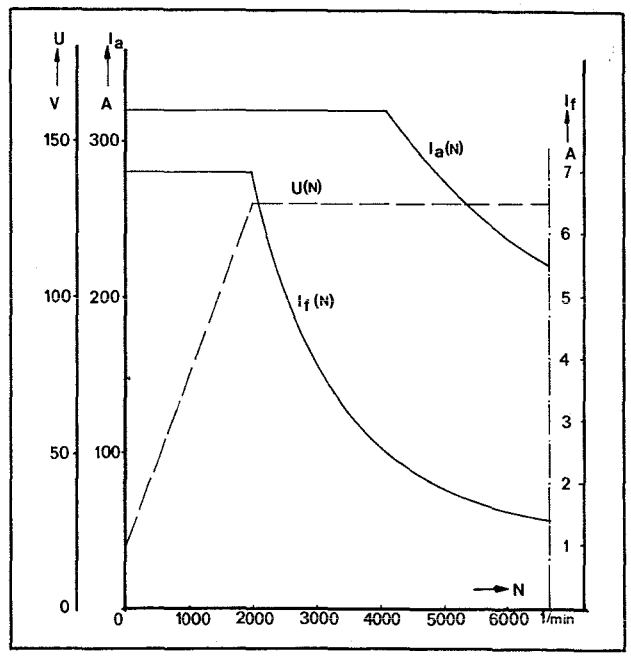

Fig. 1b The electrical performances of the 1GV1

is mostly 1 - 1.5 V, the equation of motion can be derived from (1), (2) and (3). This gives the relationship between electromagnetic torque T_e and angular speed Ω.

$$T_e = \frac{c_m \Phi_a}{R_a} (U - c_m \Omega \Phi_a) \qquad (6)$$

A general relation is found when the parameters are made dimensionless. Relating the magnitudes to their nominal values [6] we get:

$$t_e = \frac{T_e}{T_{eN}} = \frac{T_e}{c_m \Phi_{a_N} I_{a_N}} \qquad (7)$$

$$\omega = \frac{\Omega}{\Omega_N} \tag{8}$$

$$u = \frac{U}{U_N} = \frac{U}{c_m \Phi_{a_N} \Omega_N} \tag{9}$$

$$\varphi = \frac{\Phi_a}{\Phi_{a_N}} \tag{10}$$

$$r = \frac{R_a}{R_N} = \frac{R_a}{U_N / I_{a_N}} \tag{11}$$

One must be aware of the fact that U_N is defined as armature voltage under no-load conditions at nominal speed and nominal excitation. This value differs from the one given by the manufacturers for nominal motor conditions. The magitude $R_N = \frac{U_N}{I_{a_N}}$ is a fictive value which proves to be convenient once introduced. By using (6) up to (11) the general equation of motion is obtained.

$$t_e = \frac{u\varphi}{r} - \frac{\omega \varphi^2}{r} \tag{12}$$

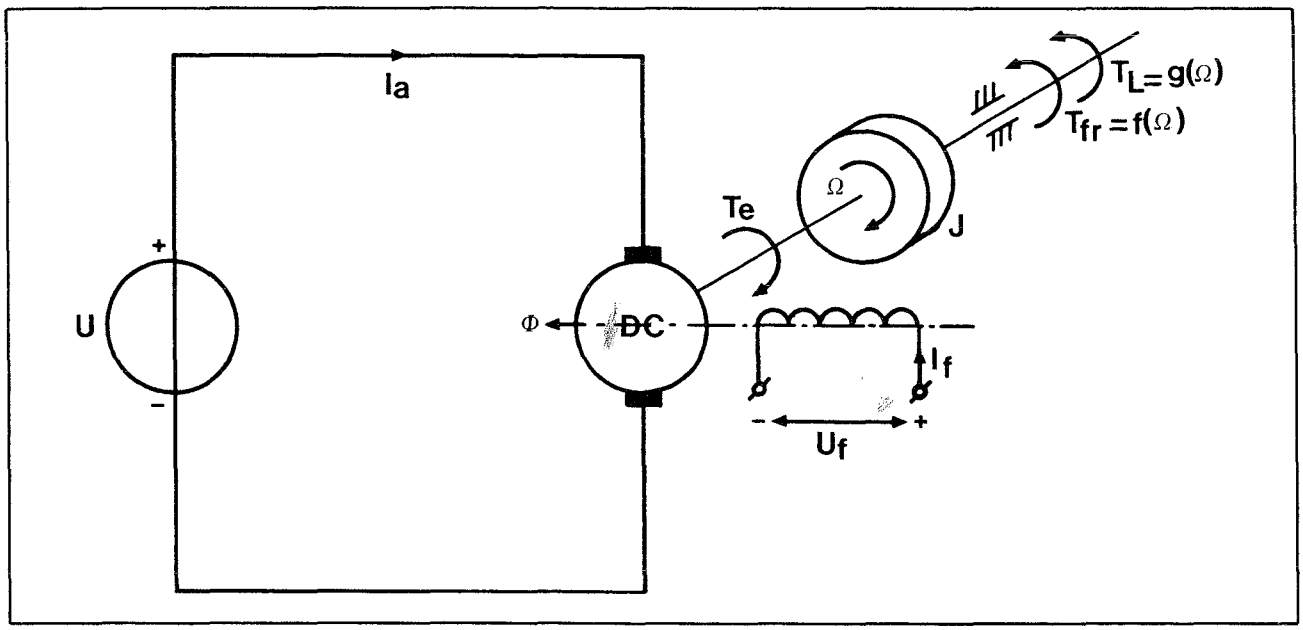

Fig. 2 Electrical drive with a DC-machine

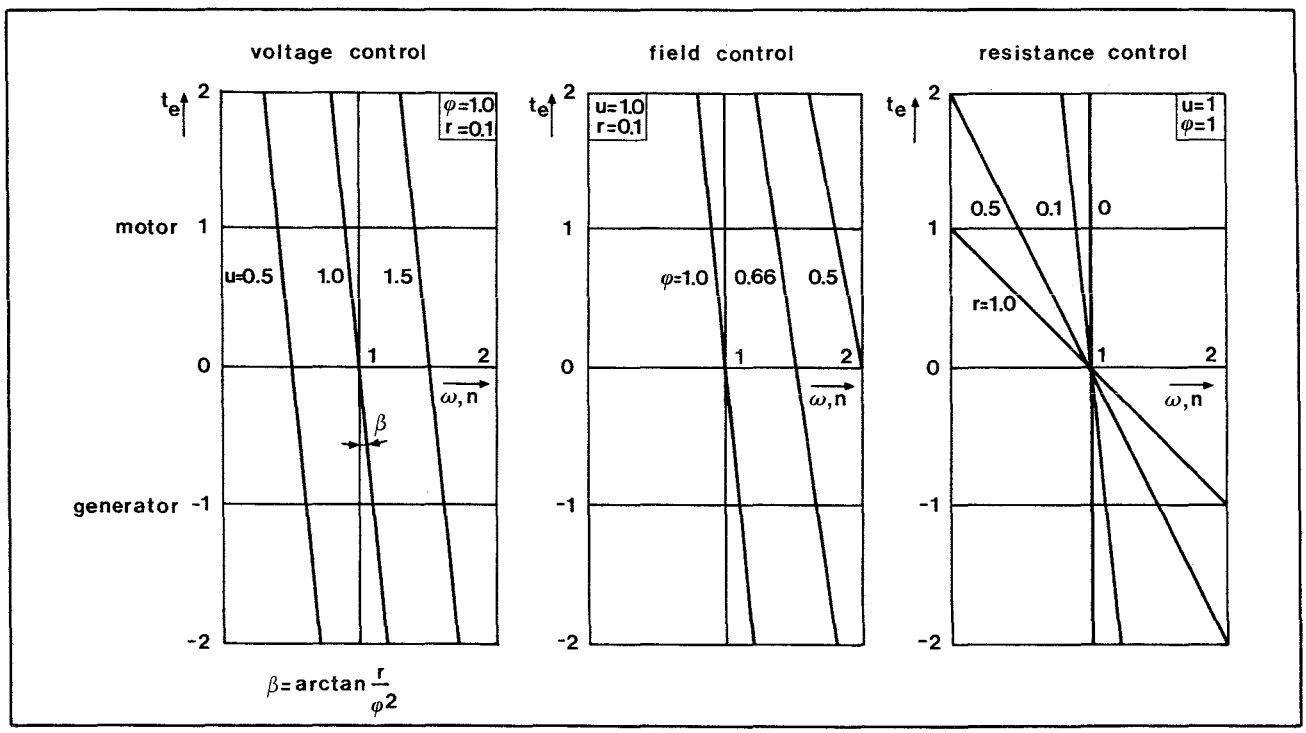

Fig. 3a Armature voltage control

Fig. 3b Field control

Fig. 3c Resistive control

Formula (12) includes three principles of affecting the torque speed curve, namely by u, φ and r. The specific influence of each of them is shown in **fig. 3a, b** and **c.**
The value r = 0,1 appears to be a quite common practice.

ad a. Speed control by armature voltage control is a very good method because of the high efficiency and the maximum torque being available at any speed. The speed range is determined by the machine parameters.

ad b. Speed control by field control offers fairly good efficiency and constant maximum output power up to high speeds, however, from very high speeds (approx. $2 \times \Omega_N$) the power is mostly limited due to commutation considerations. Compared to method **a,** field control used at voltages smaller than u = 1 will give a lower machine efficiency, because of the higher losses due to higher armature current. Besides that, the maximum power which can be converted is smaller. However, the losses in the armature controller itself are larger in a chopper than in a stepwise controller, which must be used in combination with field control, due to the fact that in the latter losses only are caused by the necessarily excitation power for electromagnetic switches. Moreover, these losses can be reduced by applying transistor choppers, such that the excitation current is limited after switching on.

ad c. Resistive speed control causes substantial energy dissipation especially at high armature current. Therefore it has a low efficiency and must be limited to the minimum.

2. SPEED CONTROL BY MEANS OF STEPWISE VOLTAGE ADJUSTMENT AND CONTINUOUS FIELD CONTROL

In the here considered drive the battery pack is devided in four blocks of 30 V each by a number of electromagnetic switches **(fig. 4).** By connecting these blocks in series and/or parallel, armature voltages of 30 V, 60 V and 120 V are obtained through which the machine speed is regulated in coarse steps. The speed can be regulated finely at each armature voltage by electronic control of the field. As the field windings are also fed from the battery pack, they had to be split in two parts in order to obtain nominal excitation current at each armature voltage.

R_v and R_p are incorporated for current limiting at low speed. Table 2 shows which switches have to be closed in a certain situation; switches which absolutely not may be closed at the same time cancel each other by normally closed interlocks.

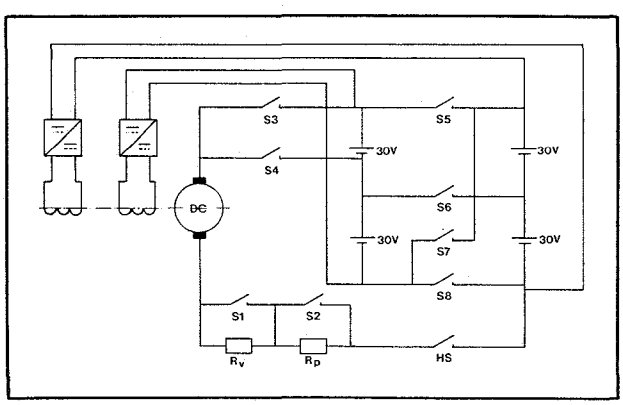

Fig. 4 Armature and field winding circuits

TABLE 2

Area	Switches in on-state								
	S1	S2	S3	S4	S5	S6	S7	S8	HS
30 V + R_v + R_p				X		X		X	X
30 V + R_v		X		X		X		X	X
30 V	X	X		X		X		X	X
60 V	X	X	X		X			X	X
120 V	X	X	X				X		X

2.1. Characteristics

The speed-torque curves for the above mentioned conditions are obtained by using (12) and the specific nominal values of the 1GV1-machine. These values are partly supplied by the manufacturer and partly determined by measurements.

$$T_{e_N} = 80\ [\text{Nm}];\ T_{S_N} = 75\ [\text{Nm}]$$

$$U_N = 124\ [\text{V}]$$

$$c_m \Phi_{a_N} = 0.54\ [\text{Wb}]$$

$$R_{a_N} = 0.83\ [\Omega]$$

$$N_{s_N} = 2200\ [\text{min}^{-1}]$$

$$R_a = 60 \cdot 10^{-3}\ [\Omega];\ r = 0.07$$

While calculating T_{e_N} no attention has been paid to the reduction of the magnetic flux Φ_a due to armature reaction and not-ideal commutation. For these reasons the effective flux will be smaller than the flux produced by the field windings only and used to derive (12).
Furthermore the torque at the machine shaft (T_S) will be smaller than T_e when the machine operates as a motor and larger when the machine operates as a generator due to iron and friction losses which depend upon speed and excitation. However, in the following we assume T_S to be linear with T_e. Furthermore nominal battery voltages are used in the characteristics and internal battery resistance is neglected.
Fig. 5 shows machine shaft torque versus machine speed and tractive effort versus car speed for armature voltages of 30 V (u = 0.24), 60 V (0.48) and 120 V (0.96) at different flux values.

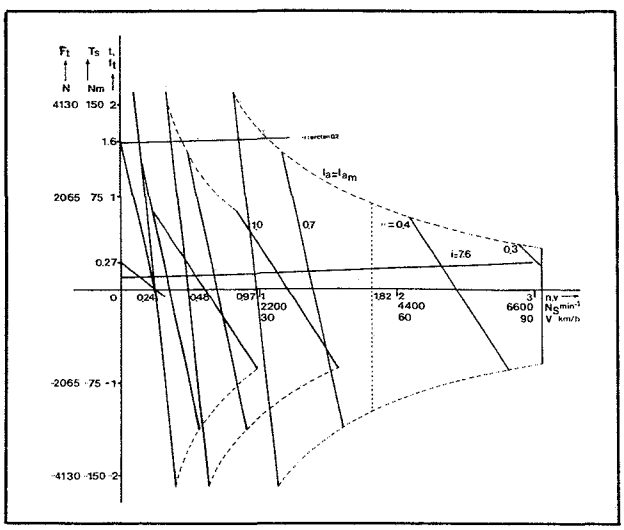

Fig. 5 Static machine characteristics and load characteristics for i = 7.6 with $\alpha = 0$ and α = arctan 0.2

Tractive effort and car speed are determined by the mechanical reduction and the wheel radius according to:

$$F_t = T_s \frac{i}{r_w} \tag{13}$$

$$V = \frac{2\pi}{60} \cdot N_s \cdot \frac{r_w}{i} \tag{14}$$

The torque is limited at all voltages by the maximum permissible armature current I_{a_M} which is constant up to $N_S = 4000$ min^{-1} ($n_S = 1.82$) and thereafter speed dependent due to the machines commutation. This dependence can be approximated by a linear function of n_S. The following equations for t_M are found.

As $|t_M| = |I_{a_M}|\,\varphi$ we get:

$$|t_M| = 2.13\,\varphi \qquad n < 1.82 \tag{15}$$

and $$|t_M| = (3.18 - 0.58n)\varphi \qquad 1.82 < n < 3.05 \tag{16}$$

The stationary load characteristics can be calculated with the wellknown formula [2]:

$$T_S = \left(\frac{1}{2}\varrho\left(\frac{2\pi}{60}\frac{r_w}{i}N_s\right)^2 A_F c_w + mg\,(f\cos\alpha + \sin\alpha)\right)\frac{r_w}{i} \tag{17}$$

The characteristic for $\alpha = 0$ and $\alpha = \arctan 0.2$ are drawn in fig. 5.

2.2. **Extra series resistors at low speeds**

In order to limit the armature current at standstill and at very low speeds to a value just high enough to produce a maximum field excitation the desired load torques, series resistors are incorporated. Two cases can be distinguished, namely:

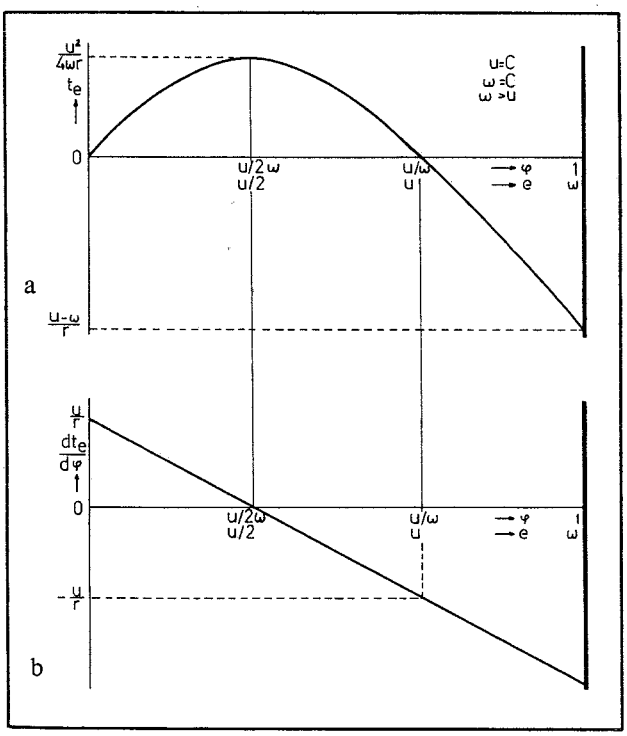

Fig. 6a EM-torque as a function of magnetic field at constant speed

Fig. 6b Transfer curve $\frac{dt_e}{d\varphi} = f(\varphi)$ at constant speed

a. Driving during a short time with a maximum torque of 120 Nm (t = 1.6), for instance in parking garages and on slopes.
b. Driving during a long time with aprox. 11 Nm (say 20 Nm; t = 0.27) while looking for a parking place or while driving in a traffic line.

The required relative resistances at standstill ($\omega = 0$) with maximum field ($\varphi = 1$) can be calculated using (12).
By taking into account the armature resistance $R_a = 0.06\,[\Omega]$ the following values for R_v and R_p are found:
$R_v = 0.065\,[\Omega]$
$R_p = 0.615\,[\Omega]$

The machine characteristics for these resistances are also shown in fig. 5. Both resistances are switched off at a machine speed of 440 min^{-1} (car speed of 6 km/h), moreover R_p is switched off when the accelerator is pushed in more then 20% ($p > 0.2$).
The switching diagram is shown in fig. 8.

2.3. **Analysis of field control at stepwise armature voltage adjustment**

In order to design a control system which is based upon field control it is essential to know certain parameters such as the transfer function $(\frac{d\,te}{d\,\varphi})$ and the position of the maximum EM-torque in the φ-n plane at different armature voltages.

2.3.1. *Quasi-stationary conditions*

For these conditions $t_e = f(\varphi)$ is analysed:

$$t_e = \frac{\varphi}{r}(u - \varphi\omega)$$

1. The zeros are found at $\varphi = 0$ and $\varphi = \frac{u}{\omega}$.

2. The maximum EM-torque will be produced when the total voltage drop across the armature circuit resistances equals the back E.M.F. :

$i_a r = \varphi\omega = \frac{u}{2}$. Its magnitude is: $t_{e_M} = \frac{u^2}{4\omega r}$.

3. The minimum EM-torque (maximum torque as generator) is limited by the maximum value of the field ($\varphi = 1$) and has a magnitude of:

$$t_{e_M} = \frac{1}{r}(u - \omega).$$

The EM-torque as a function of φ and e at constant armature voltage u is outlined in **fig. 6.** Also shown is the static transfer curve $\frac{dt_e}{d\omega} = f(\varphi, e)$.

Fig 6. shows that for small back E.M.F. (i.e. $e < \frac{u}{2}$) an increase of the field will result in higher EM-torque and for high back E.M.F. (i.e. $e > \frac{u}{2}$) in lower EM-torque.
The latter is almost always the case in motor applications of the DC-machine, however, not in the one considered here.

All points in the φ-ω plane, at which under motor conditions the EM-torque is maximum, lie on a orthogonal hyperbole which is determined by the armature voltage, i.e.

$$\varphi\omega = \frac{u}{2} = C$$

The constant C for the armature voltages 30, 60 and 120 V is respectively: 0.12, 0.24 and 0.48.
Another important factor involved, is the magnitude of the armature current which must be held within certain limits. Curves for maximum permissible armature current under motor conditions as well as under generator conditions are also orthogonal hyperboles:

$$\varphi\omega = u - i_{a_M} \cdot r \qquad (19)$$

with $i_{a_M} = \pm 2.13$ for $\omega < 1.82$

and $i_{a_M} = \pm (3.18 - 0.58\,\omega)$ for $1.82 < \omega < 3.05$

All the curves mentioned and the one for armature current equal to zero are drawn in **fig. 7** for the distinct voltage levels and armature circuit conditions.

The criteria for changeover between armature voltage levels under motor conditions differ from those under generator conditions.
– Changeover under motor conditions ($T_s > 0$):
As changeover must occur while the armature current is zero, the machine speed must be high enough to get a back E.M.F. equal to the next voltage level at maximum field ($\varphi = 1$).
This means $\omega = u$. The following values are found: (20)

$n_{30 \rightarrow 60} = 0.48$; $N_{s30 \rightarrow 60} = 1056\ \text{min}^{-1}$

$n_{60 \rightarrow 120} = 0.96$; $N_{s60 \rightarrow 120} = 2112\ \text{min}^{-1}$

– Changeover under generator conditions ($T_s > 0$):
In this case it is important to keep the breaking torque which *can* be produced as high as possible. This means that the maximum power delivered by the machine just after switching must be equal to the maximum power before switching, taking into account the field limit $\varphi = 1$ befor switching and the armature current limit $i_a = 2.13$ after.
From this it follows that:

$$n = \frac{u_H}{2} + \sqrt{\left(\frac{u_H^2}{4} + i_{a_M} r\left(\frac{u_H}{2} + i_{a_M} r\right)\right)} \qquad (21)$$

Herein is u_H the highest of the two involved armature voltages at a certain switching point.

Hence $n_{120 \rightarrow 60} = 1.05$; $N_{s120 \rightarrow 60} = 2310\ \text{min}^{-1}$
and $n_{60 \rightarrow 30} = 0.58$; $N_{s60 \rightarrow 30} = 1276\ \text{min}^{-1}$

Figure 7 gives a complete survey of the requirements of the field control system, while figure 8 shows the exact situation of switching points at certain armature circuit conditions. The following conclusions with respect to this control system can be drawn for the distinct areas:

Area I: $U = 30$ V; $R \geq 0.125\ \Omega$; $-320\ \text{A} < I_a < 320\ \text{A}$.
– The maximum permissible armature current cannot be exceeded.
– The transfer function $\frac{dt_e}{d\varphi}$ is positive except for $260 < N_s < 440$, so that the field in this range is limited according to $\varphi = -2.27.10^{-3} N_s + 1.60$.

Area II: $U = 30$ V; $R = 0.06\ \Omega$; $-320\ \text{A} < I_a < 320\ \text{A}$.
– The armature current must be limited in both positive and negative direction.

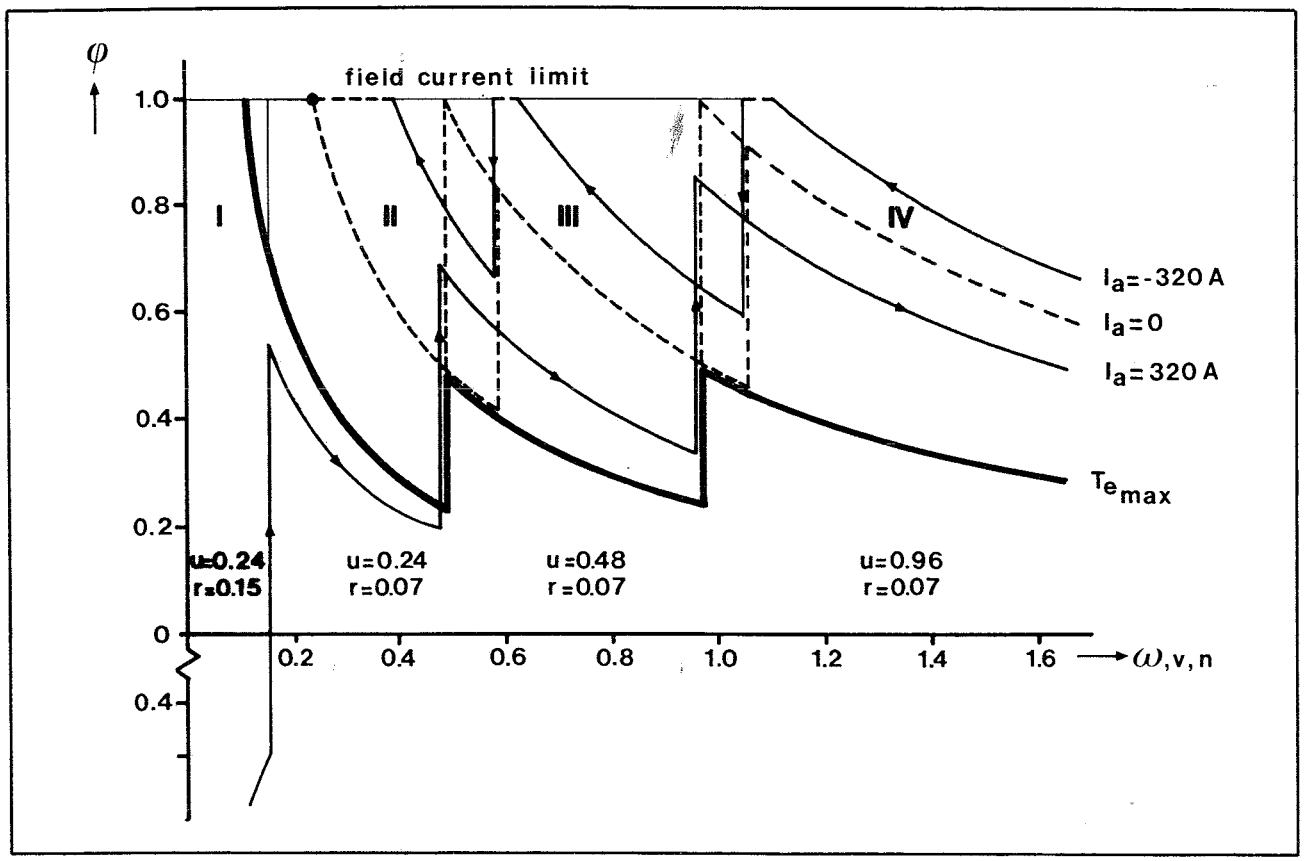

Fig. 7 Notching curves for maximum EM-torque and maximum current in the φω-plane

– In the largest part of the area the transfer function $\frac{dt_e}{d\varphi}$ is negative. During testing it appeared to be satisfactory to consider $\frac{dt_e}{d\varphi}$ negative all over the area.

Area III: U = 60 V; R = 0.06 Ω; $-320\ A < I_a < 320\ A$.
– The armature current must be limited in both directions.
– The transfer function $\frac{dt_e}{d\varphi}$ is negative all over the area.

Area IV: U = 120 V; R = 0.06 Ω; $-I_{a_M} < I_a < I_{a_M}$; $I_{a_M} = f(N)$; conditions: Identical to area III.

As the exact situation of the curves depend on the battery condition in such a way that under poor battery conditions the curve for maximum torque will possibly become higher situated in the φω-plane than the maximum motor current curve, it is necessary to take precautions in order to prevent the torque from falling to a very low value. Therefore the field in area II, III and IV is kept above the value of 0.2.

2.3.2. *The dynamic behaviour of the separately excited DC-machine with field control*

In the preceding pages field control has been regarded under quasi-stationary conditions which means that changes occur so slowly that the system, the electrical as well as the mechanical part, can follow immediately. The system behaviour under these circumstances is the most important for EV-applications, however, with respect to system design also the dynamic behaviour is important [1], [5] and [8].

The transfer function $\frac{T_e}{\varphi}$ or $\frac{T_e}{U_f}$ can only by determined for small signals around a working point due to the non-linearity of machine equations and the load characteristic. The following transfer function can be derived in the Laplace-domain, assuming a linear relationship exists between Φ_s and Φ_a.

$$H(s) = L\left\{\frac{T_e}{U_f}\right\} = \frac{-2c_1\Omega_{a_o}c_m(E_o - I_{a_o}R_a)}{2c_1\Omega_{a_o}R_a + c_m^2\Phi_o^2} \cdot \frac{(1+\frac{J}{2c_1\Omega_{a_o}}s)(1-\frac{I_{ao}L_a}{E_o - R_aI_{a_o}}s)}{(\frac{JL_a}{2c_1\Omega_{a_o}R_a + c_m^2\Phi_o^2}s^2 + \frac{JR_a + 2c_1\Omega_{a_o}L_a}{2c_1\Omega_{a_o}R_a + c_m^2\Phi_o^2}s + 1)(\frac{R_f}{L_{fo}} + s)} \quad (22)$$

Where: $\Omega_o = \frac{i}{r_w}V_o$

$E_o = c_m \Phi_o \Omega_o$

$c_1 = \frac{1}{2}\varrho A_F c_w \frac{r_w^3}{i^3}$

$J = \frac{r_w^2}{i^2}\lambda m$

λ is a constant necessary to bring into account the rotating parts of the drive. The parameters with subscript "0" refer to the chosen working point. With the wellknown techniques from control engineering it is possible to determine the response to a step input signal $U_{f\sim}$.

It appears that:
– the final value of the response has a sign *opposite* to that of $U_{f\sim}(E_o - I_{a_o}R_a)$ (see also fig. 6a.).
– the differential coefficient $\frac{dT_e}{d\tau}$ at time $\tau = 0$ has the *same* sign as that of the disturbance $U_{f\sim}$.

This means that when $E_o - I_{a_o}R_a > 0$ the system at first shows an inverse response (see **fig. 9**). The transfer function has a zero in the right part of the complex s-plane and is called a *nonminimum phase-shift transfer function.*
The physical explanation for this phenomenon is the existance of the electrical inertia of the armature, through which the transient at the beginning is determined by the field only.

3. REALISATION OF THE CONTROL SYSTEM

In principle an armature current or field control is sufficient to control speed, acceleration and regenerative breaking. However, due to the speed dependence of the field, the accelerator or brake pedal position would need to be readjusted continually in order to keep the desired acceleration or deceleration. By applying an extra torque control loop, the driving or breaking torque is kept constant as far as the armature or field current limits are not exceeded.

In the area where the series resistors are incorporated in the armature circuit and hence $\frac{dt_e}{d\varphi} > 0$, the field is controlled straightaway by the accelerator pedal signal. Fig. 10a, and b shows the block diagrams of the distinct control systems.

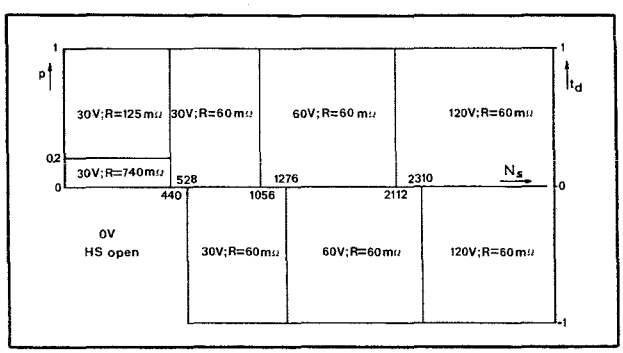

Fig. 8 Switching diagram

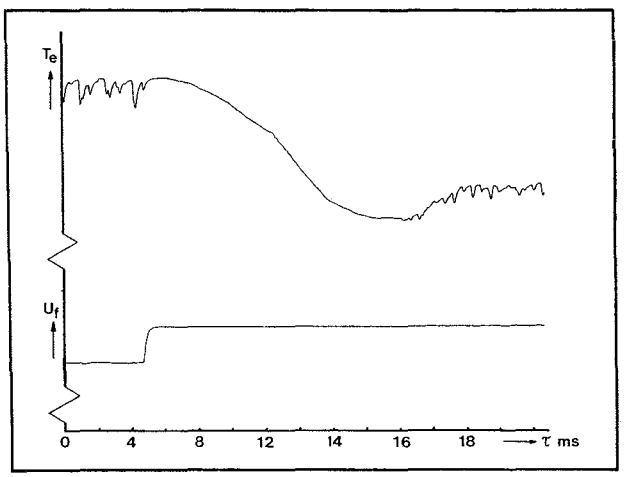

Fig. 9 Torque response to step input field winding voltage

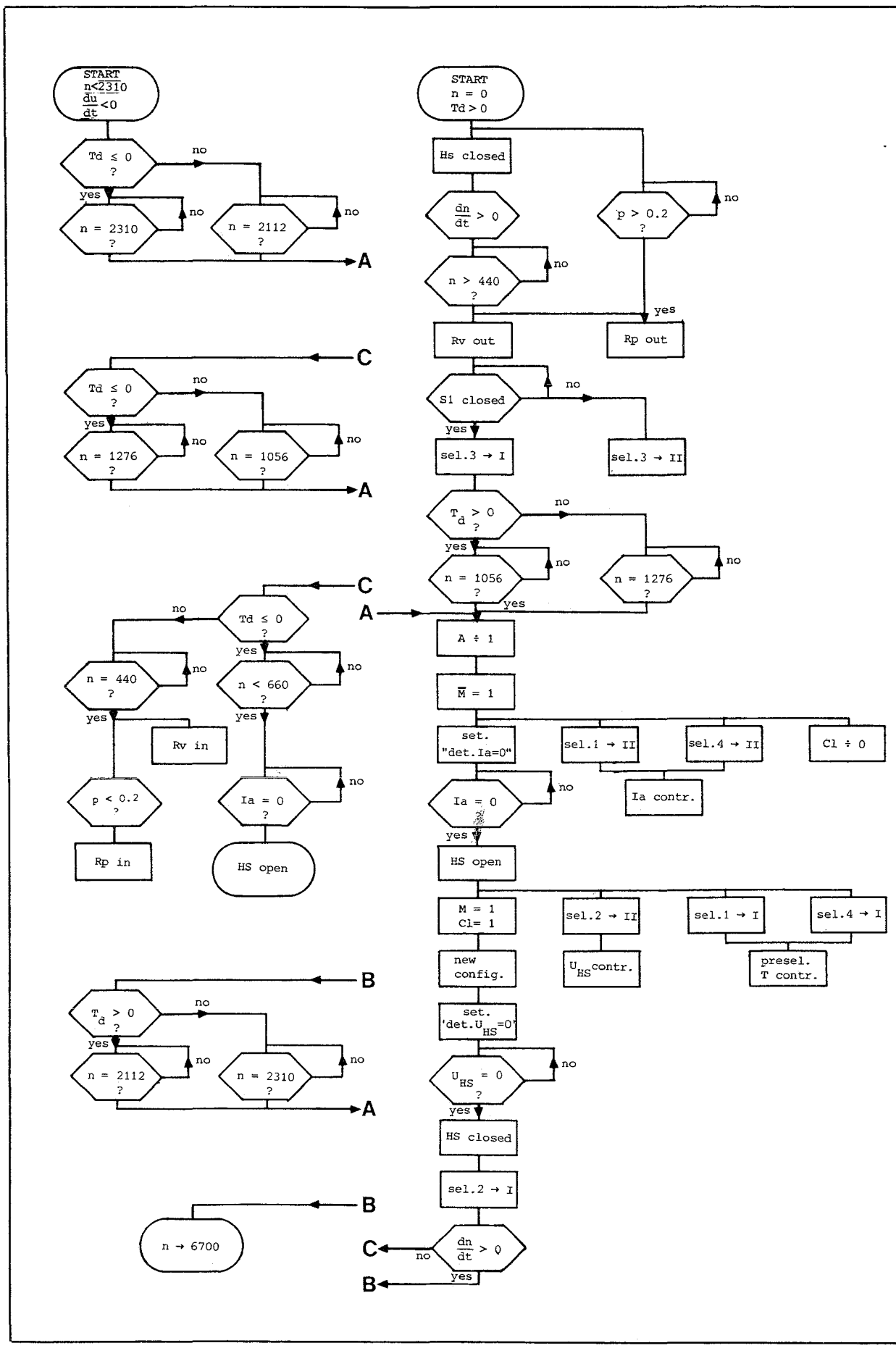

Fig. 14 Flow chart for accelerating and decelerating

3.1. Field current controllers

The field current controllers are two-quadrant choppers implemented with power MOSFETs (see **fig. 11a**). Due to the fact that the excitation voltage can be reversed, current changes can be accomplished with the same speed in both directions (see **fig. 11b**).

For a fast decrease of the field current, the energy stored in the field windings will be fed back into the battery via the diodes D1 and D2. The frequency of the PWM-signal is 400 Hz which is high enough to get a smooth current at a given field coil time constant of 100 ms.
The average excitation voltage and, under stationary conditions, also the average current is proportional to the control voltage applied to the PW-modulator (**fig. 11c**).

3.2. Measurement of the field

Due to the saturation of the magnetic circuit and hence non-linear relation between I_f and Φ_s, the field current cannot be used straightaway to determine the instantaneous EM-torque. Although, if the hysteresis is neglected, this function can be approximated quite accurately using the method of least squares, in practise it appeared to be satisfactory to make an even coarser approximation with three straight lines which remain all within the hysteresis curve (**fig. 12**).
Based upon this approach the flux value is obtained electronically from the field current.

4. FLOW CHART AND BLOCK DIAGRAM OF VOLTAGE ADJUSTING AND FIELD CONTROL SYSTEM

In order to change armature voltage under no-current conditions the current before *opening* the main switch and the vol-

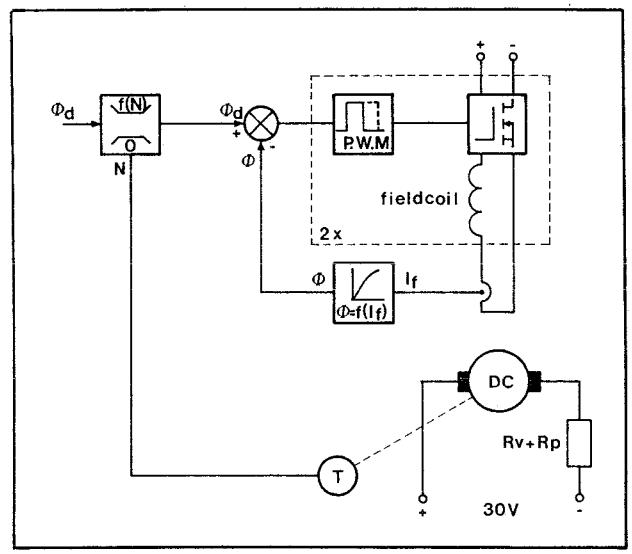

Fig. 10a Field control in the area U = 30 V; R ≥ 125 mΩ

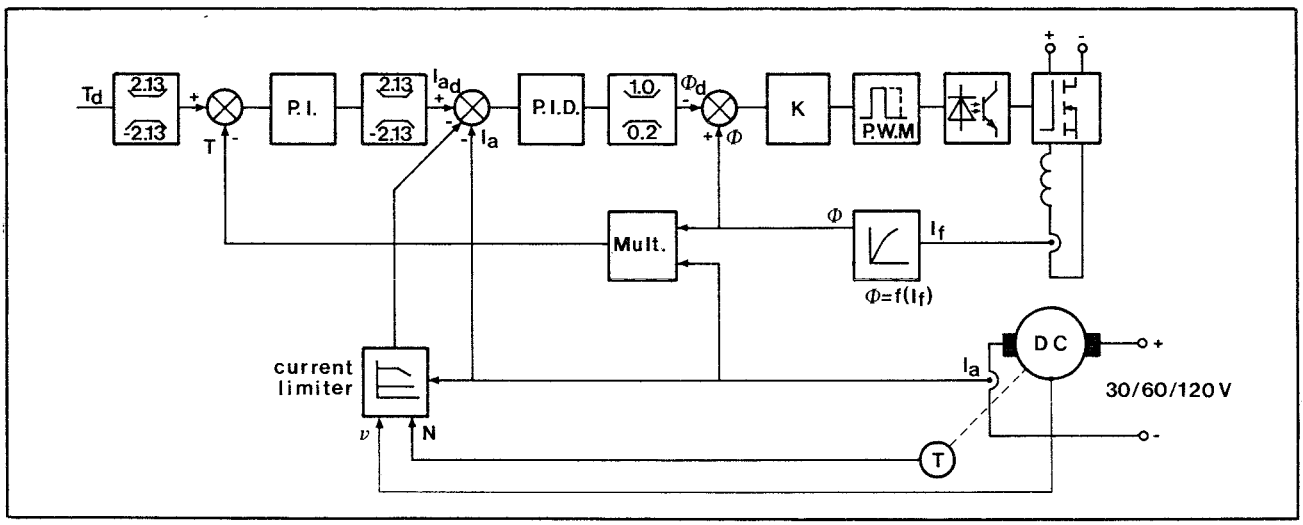

Fig. 10b Torque control in the areas U = 30, 60 and 120 V; R = 60 mΩ

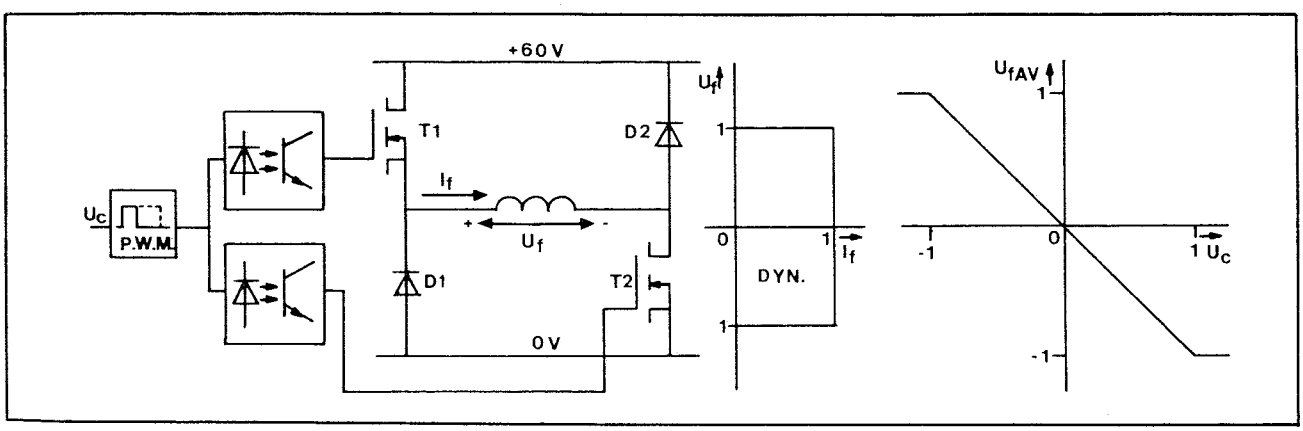

Fig. 11a Field current chopper

Fig 11b Two quadrant operation

Fig. 11c Excitation voltage vs. control voltage

Fig. 15 Block diagram

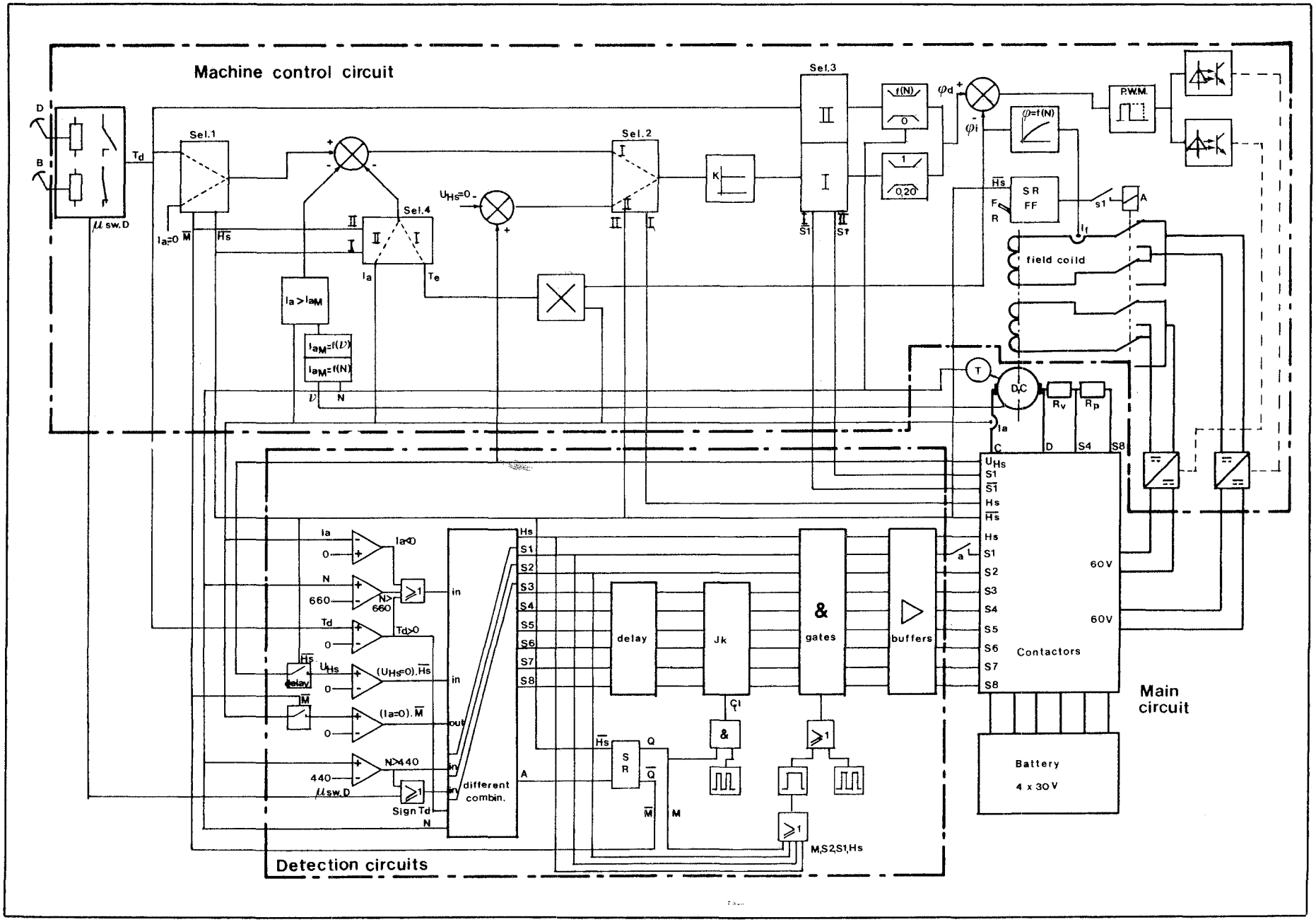

tage across the main switch before *closing* it in the new state, are forced to zero.
Due to this program the field control operates successively under torque-, current-, and voltage control. The entire program is a complex structure which can best be understood by following the flow chart of **fig. 14,** together with the block diagram of **fig. 15. Fig. 13** shows the voltage across the main switch, the armature current and the field current during switching.

5. CONCLUSIONS

The conclusions drawn from the obtained test-bench results can be summarized as follows.
– It is possible to build a convenient speed control based upon a conventional circuit concept with use of modern control electronics.
– The control concept is probably very suitable to implement with microprocessor technology, which means that prices can be acceptable in larger series.
– The relatively low torque-armature current ratio, due to the field weakening, can be regarded as a disadvantage of this speed control.

6. ACKNOWLEDGEMENTS

The author wishes to express his thanks to professor J.A. Schot for reading the manuscript and to acknowledge his gratitude to Messrs. Barten, v. d. Boomen and Kremer, who are responsible for much of the realisation of this project.

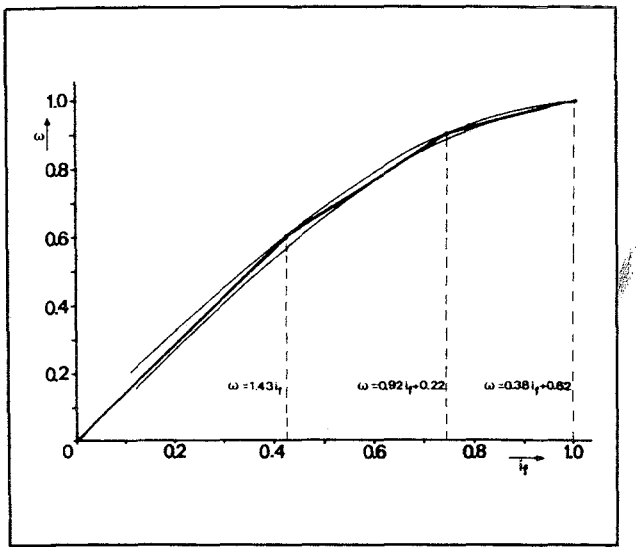

Fig. 12 Linear approximation of $\Phi_s = (I_f)$

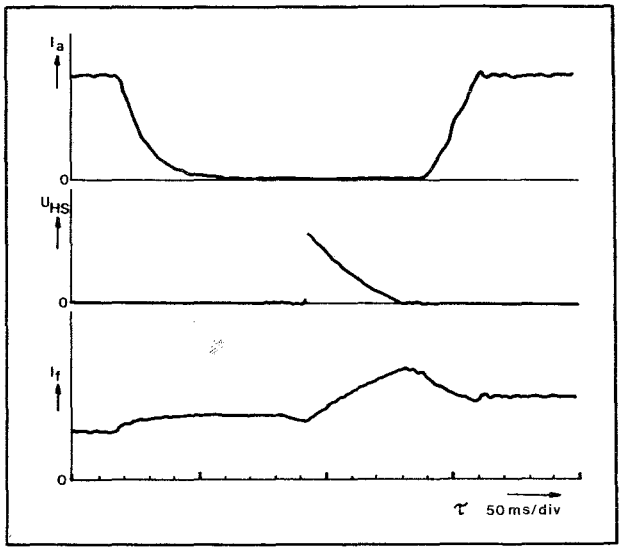

Fig. 13 Armature current, voltage across main switch and field current vs. time during switching to a higher voltage

LIST OF SYMBOLS AND SUBSCRIPTS

A_F Front surface of car.
c_m Machine constant.
c_w Streamline constant.
E Back E.M.F.
e Normalized E.M.F.
F_t Tractive effort.
f Friction constant.
g Gravity constant.
H(s) Complex transfer function.
HS Main switch.
I_a Armature current.
I_f Excitation current.
i_a Normalized armature current.
i Mechanical reduction.
J Mechanical inertia.
L_a Armature inductance.
L_f Field coil inductance.
m Mass of the vehicle.
N_s Machine shaft speed.
p Accelerator position.
R Total armature circuit resistance.
R_a Armature resistance.
R_f Field coil resistance.
R_N Nominal armature resistance $\frac{U_N}{I_{a_N}}$.
R_p Parking resistor
R_v Series resistor.
r Normalized armature circuit resistance.
r_w Wheel radius.
S Switch.
s Laplace operator.
T_s Machine shaft torque
T_e Electromagnetic torque.
T_{fr} Friction torque.
T_L Load torque.
t_e Normalized EM-torque.
U Armature voltage.
U_b Voltage drop across brushes.
U_f Field coil voltage.
u Normalized armature voltage.
V Vehicle speed.
v Normalized vehicle speed.
α Slope angle.
λ Constant.
ν Field winding temperature.
ϱ Specific air density.
τ Time.
Φ_a Enclosed stator flux.
Φ_s Stator flux.
φ Normalized flux $\frac{\Phi_a}{\Phi_N}$
ω Normalized angular speed.
Ω_s Angular machine shaft speed.

Additional subscripts

AV Average value.
L Laplace domain.
M Maximum.
m Minimum.
N Nominal.
o Working point.
$\sim$ Small signals.

REFERENCES

[1] Cool, J. C., Schijf, F. J. Viersma, T. J., Regeltechniek. Elsevier, Amsterdam/Brussel 1979.

[2] Dongen, L. A. M. van, 'Aandrijflijnen voor elektrische voertuigen' Rapportnr. WV 155-043, T.H. Eindhoven 1979.

[3] Dongen, L. A. M. van, Graaf, R. van der, 'The Eindhoven Experimental Vehicle: Vehicle Design and Drive Train', Drive Electric Amsterdam 1982.

[4] Dongen, L. A. M. van, Graaf, R. van der, Visscher, W. H. M., 'Theoretical Prediction of Electric Vehicle Energy Consumption and Battery State-of Charge During Arbitrary Driving Cycles', EVC No. 8115, EVC Symposium VI Baltimore, Maryland

[5] Dorf, R. C., Modern Control Systems, third edition. Addison-Wesley, Reading Massachusetts 1980

[6] Jong, H. C. J. de, Kreek, J. van der, 'De statische karakteristieken van de gelijkstroomcommutatormachine' Lecture notes EM-3615-0, group Electromechanics, T.H. Eindhoven

[7] Koumans, W. A., 'Electric car project of the Eindhoven University of Technology' PPL Conference Publication number 14, pp 87-90

[8] Pfaff, G., Reglung Elektrischen Antriebe I: Eigenschaften, Gleichungen und Strukturbilder der Motoren R. Oldenbourg Verlag, München und Wien 1971

[9] Siemens, A. G., Gleichstrom-Fahrmotor 1GV1: Technische Beschreibung.

[10] Visscher, W. Dongen, L. A. M. van, 'Battery State-of Charge Model for Driving Cycle Operation'. Drive Electric Amsterdam 1982